Environmental Science Advances

ROYAL SOCIETY OF CHEMISTRY

PAPER

View Article Online
View Journal | View Issue

Cite this: *Environ. Sci.: Adv.*, 2024, **3**, 1598

A hybrid anion exchanger with nanoscale zero valent iron for trace hexavalent chromium removal from drinking water†

Annabel L. Mungan, [a] Elizabeth A. Hjelvik, [b] Anthony P. Straub [abc] and Julie A. Korak *[ac]

Hexavalent chromium, Cr(VI), is a human carcinogen that occurs in groundwater worldwide. While not federally regulated in the USA, the State of California has approved a new Cr(VI) maximum contaminant level at 10 μg L^{-1}, expected to go into effect fall 2024. This study synthesizes, characterizes, and verifies performance of a hybrid strong base anion exchanger with nanoscale zero valent iron (NZVI-resin) for trace Cr(VI) removal from drinking water. NZVI-resin was synthesized by exchanging tetrachloroferrate ion ($FeCl_4^-$) onto the resin prior to sodium borohydride ($NaBH_4$) reduction. The impact of important synthesis variables was identified, including reagent concentrations and molar ratios, solvent selection, temperature, and drying procedure. Material characterization techniques (*e.g.* SEM-EDS and XPS) determined NZVI presence and elemental distribution on the resin surface. Our work showed a 360% increase in treated water throughput using NZVI-resin compared to unmodified resin for trace Cr(VI) removal in column experiments. This work presents a broad assessment of the material characteristics of NZVI-resin, discusses the limitations of batch tests, and describes operational challenges for Cr(VI) treatment.

Received 30th June 2024
Accepted 12th September 2024

DOI: 10.1039/d4va00246f

rsc.li/esadvances

Environmental significance

Hexavalent chromium is a toxic element and may be found in water sources used for drinking water from either naturally occurring geological formations or anthropogenic contamination. Ion exchange is one treatment technology that can selectively remove hexavalent chromium, but the process is inefficient for source waters with high concentrations of sulfate. This study synthesized and tested a hybrid resin that embeds reactive iron nanoparticles in commercial ion exchange resin to improve chromium removal. In addition to demonstrating the advantages of this hybrid resin, this study also highlights opportunities by identifying challenges associated with material characterization and demonstration testing.

1 Introduction

Chromium occurs naturally as a mineral in the earth's mantle.[1] It often exists in the form of trivalent chromium (Cr(III)) within ultramafic- and serpentinite-derived soils and rock, which through natural processes can be oxidized to hexavalent chromium (Cr(VI)) in the groundwater, particularly in alkaline, oxic conditions.[2,3] Anthropogenic activities, such as groundwater pumping and nutrient pollution, are also correlated with accelerated Cr(III) oxidation to Cr(VI).[2] Naturally elevated concentrations of aqueous Cr(VI) exceeding 50 μg L^{-1} in groundwaters have been reported worldwide, including California, Arizona, Mexico, Brazil, Italy, New Caledonia, Australia, and India.[4] Cr(VI) may also enter the water supply through industrial processes, including paint dying, plastic making, leather tanning, industrial water cooling, and metal finishing.[5,6] Since chromate (CrO_4^{2-}) mimics the structure of phosphate and sulfate salts, it is readily taken up by biological cells.[7] Cr(VI) has been shown to be carcinogenic both by inhalation and by ingestion, such as through drinking water.[8,9] Due to its toxicity and occurrence in groundwater sources, Cr(VI) is a contaminant of interest for drinking water treatment.

As of 1992, the United States Environmental Protection Agency (USEPA) has regulated total chromium (Cr(III) and Cr(VI) combined) at 100 μg L^{-1}. The European Union (EU) regulates total chromium at 50 μg L^{-1} and plans to lower this standard to 25 μg L^{-1} by 2036.[10] In 2014, California (USA) issued a drinking water maximum contaminant level (MCL) of 10 μg L^{-1} Cr(VI), motivating the industry to invest in research developing full-scale technologies for Cr(VI) treatment. By 2017, however, the regulation was rescinded due to a lack of economical treatment solutions.[11] In March 2022, California re-proposed this 10 μg L^{-1}

[a]*Department of Civil, Environmental, and Architectural Engineering, University of Colorado Boulder, Boulder, Colorado, USA. E-mail: Julie.Korak@colorado.edu*

[b]*Materials Science and Engineering Program, University of Colorado Boulder, Boulder, Colorado, USA*

[c]*Environmental Engineering Program, University of Colorado Boulder, Boulder, Colorado, USA*

† Electronic supplementary information (ESI) available. See DOI: https://doi.org/10.1039/d4va00246f

Cr(VI) MCL, which is expected to take effect Fall 2024 with a compliance phasing approach based on number of service connections.[12] According to the USEPA's Second Six-Year Review from 1998–2005, 8623 water supplies in the United States have Cr(VI) concentrations above 10 μg L^{-1}, with 681 water supply entry points in the state of California. Of the 8623 water supplies, 54% of systems serve populations less than 1000 people and 83% of systems serve populations less than 10 000 people, often through small groundwater-fed pump stations. The highest occurrence of Cr(VI) is found in California, Arizona, and Nevada.[13] Economical technologies for Cr(VI) removal are therefore imperative, especially modular solutions for decentralized groundwater systems in California communities.

The USEPA lists three best available technologies (BATs) for Cr(VI), which are those technologies found to be effective to decrease Cr(VI) concentrations below 1 μg L^{-1} at full-scale. These technologies are reverse osmosis (RO), reduction–coagulation–filtration (RCF) by ferrous salts, and ion exchange (IX).[14] While RCF is more viable than IX for high sulfate waters, it is disadvantageous due to its larger footprint, need for a sewer connection, and constant chemical addition.[15]

Strong base anion exchange (SBA-IX) is a widely used technology for Cr(VI) treatment in drinking water. SBA-IX uses commercially synthesized resin consisting of a polymeric skeleton (*e.g.*, polystyrene or polyacrylate) that is crosslinked with divinylbenzene (DVB) and can be synthesized with two different morphologies. Gel resin (4–10% DVB) is translucent, has high water content, and has a large ability to swell and shrink. Macroporous resin (20–25% DVB) is opaque, has lower water content, and has a lower ability to swell and shrink.[16] Anion exchange resins have positively charged functional groups, which can exchange anions onto the resin by displacing other counterions. At full-scale, SBA-IX systems feed influent water through packed-bed contact vessels containing resin, which remove CrO_4^{2-} from water. When resin particles reach their maximum capacity for CrO_4^{2-}, multiple-use resins can be regenerated by sending a concentrated regenerant solution, typically 10–14% (w/w) sodium chloride (NaCl), through the contact vessels, and collecting the waste brine.[17] Advantages of SBA-IX include simple process design, high selectivity for Cr(VI), and lack of sludge production.

Disposal of waste brine is one of the greatest challenges for IX processes, which are often operated at decentralized groundwater wells without access to a centralized wastewater system. In addition, when the target constituent (*e.g.*, CrO_4^{2-}) is hazardous, the brine produced during regeneration can have high concentrations of hazardous materials, with reported concentrations of CrO_4^{2-} ranging from 12–320 mg L^{-1}.[18] These hazardous brines must not only be hauled offsite, but also disposed of at special hazardous waste facilities.[18] Operating costs for SBA-IX resin were estimated as $1.16 USD/1000 US liquid gallons of treated water in 2018, primarily due to disposal costs.[19]

Because waste disposal is so costly, maximizing the capacity of SBA-IX resin for CrO_4^{2-} is crucial. Several anions compete with CrO_4^{2-}, including sulfate (SO_4^{2-}), nitrate (NO_3^-), chloride (Cl^-), and bicarbonate (HCO_3^-). Other co-occurring oxyanionic contaminants can include arsenic, vanadium, and uranium.[20] While both are divalent, SO_4^{2-} occurs at concentrations thousands of times higher than CrO_4^{2-}. Thus, SO_4^{2-} is the primary driver of SBA-IX resin capacity for trace Cr(VI) removal. For instance, for a Cr(VI) concentration of approximately 15 μg L^{-1}, an increase in SO_4^{2-} from 35 to 49 mg L^{-1} decreased the expected throughput for A600E from 19 000 to 12 500 bed volumes (BV).[21] By increasing resin capacity and/or selectivity for Cr(VI) over SO_4^{2-}, SBA-IX can be improved as a drinking water treatment technology for Cr(VI) removal, specifically for high-sulfate groundwaters.

Hybrid ion exchange (HIX) is a class of ion exchange materials that disperses metal or metal oxide nanoparticles within ion exchange resin.[22] In other applications, HIX has demonstrated higher capacity, exploiting the sorption capacity of the metal adsorbent and the ion exchange capacity of the resin. Leveraging the Donnan membrane principle, resins have ion-permeable, solid–liquid interfaces that favor the enrichment of trace ions in the resin phase over the aqueous phase. Therefore, in solutions with trace levels of target ions, the HIX resin can exhibit faster kinetics than metal nanoparticles on their own.[22,23]

Nanoscale zero valent iron (NZVI) is elemental iron (Fe^0) synthesized as nanoparticles of approximately 60–70 nm, which demonstrates significantly increased surface area for reactions and adsorption as opposed to powder or granular iron.[24,25] Elemental iron is abundant, inexpensive, and non-toxic, although a secondary MCL of 0.3 mg L^{-1} exists for iron in the USA due to the reddish color and metallic taste. NZVI is an effective reactive sorbent for *in situ* groundwater remediation of inorganic contaminants including nitrate, perchlorate, selenate, arsenate, arsenite, and chromate.[26–28] However, when used on its own, NZVI has a number of drawbacks. Because of its high reactivity, NZVI can lose capacity by surface oxidation before the particles come into contact with target species.[24] Due to magnetic and van der Waals forces, NZVI is also prone to aggregation, which reduces its surface area.[29] Thus, impregnation of NZVI on substrates, such as polymers and porous carbon, may effectively slow surface oxidation and prevent aggregation.

NZVI-impregnated anion exchange resins are formed in three steps. First, tetrachloroferrate anion ($FeCl_4^-$) is formed in an alcohol solution with excess chloride, according to eqn (1):[30]

$$FeCl_3 + Cl^- \leftrightarrow FeCl_4^- \quad (1)$$

Next, $FeCl_4^-$ is exchanged onto the anion exchange resin following eqn (2). The overbar represents the resin phase, and R^+ represents the charged functional groups fixed in the resin phase.

$$\overline{R^+Cl^-} + FeCl_4^- \leftrightarrow \overline{R^+FeCl_4^-} + Cl^- \quad (2)$$

Third, ferric iron is then reduced to Fe^0 using sodium borohydride ($NaBH_4$), which is a readily available and effective reducing agent,[25] following eqn (3):

$$4\overline{FeCl_4^-} + 3BH_4^- + 9H_2O \rightarrow 4Fe^0(s) + 3H_2BO_3^- + 12H^+ + 16Cl^- + 6H_2(g) \quad (3)$$

Table 1 Previous studies using NZVI HIX for Cr(VI) removal

Study	Resin	Experiment	[Cr(VI)] (mg L^{-1})	pH	Application
31	Cationic	Batch	20–40	3–9	Industrial wastewater treatment
32	Cationic	Batch	5–25	2.7–8.5	Contaminated water
33	Anionic	Batch	20–150	3–10	Industrial wastewater treatment
34	Cationic	Column	5	4.9	Industrial wastewater treatment
35	Cationic	Column	0.5–5.2	2–7.5	Industrial wastewater treatment
This study	Anionic	Batch	175	8–9	Groundwater-sourced drinking water treatment
		Column	0.091		

Table 1 shows that no prior studies have investigated use cases for NZVI impregnated resins that are applicable to drinking water treatment. Applications span both industrial wastewater treatment and remediation of polluted groundwater. At pH ranges and trace concentrations of Cr(VI) relevant to drinking water; however, studies are absent, driven largely by the absence of a low MCL value in drinking water. No other studies have yet examined removal of Cr(VI) by NZVI-impregnated on SBA-IX in both continuous flow column tests and at trace contaminant concentrations. Further details on prior studies are included in ESI† Text 1.3.[31–36]

Given the newly proposed California MCL of 10 μg L^{-1} Cr(VI), our work aims to disperse NZVI within SBA-IX resin for trace Cr(VI) removal from drinking water. We have synthesized, characterized, and tested the performance of NZVI on SBA-IX resin in batch and fluidized bed experiments. In addition, we have critically considered the viability and practicality of this HIX technology for full-scale operation, including selectivity over background constituents, durability, and impact on pH and water chemistry of treated water.

2 Methods

2.1 Materials

All chemicals were analytical reagent grade. Solids used included ferric chloride ($FeCl_3 \cdot 6H_2O$), sodium borohydride ($NaBH_4$), 1,5-diphenylcarbazide ($C_{13}H_{14}N_4O$), sodium sulfate (Na_2SO_4), sodium chloride (NaCl), sodium nitrate ($NaNO_3$), and sodium bicarbonate ($NaHCO_3$). Solutions used included absolute ethanol (C_2H_6O), acetone, hydrochloric acid (HCl), sulfuric acid (H_2SO_4), nitric acid (HNO_3), 1000 mg L^{-1} sodium chromate (Na_2CrO_4), and 5% w/v sodium chromate tetrahydrate ($Na_2CrO_4 \cdot 4H_2O$). Four resins were tested, but only results using a strong base anion exchange resin, A600E/9149 from Purolite®, were successful and therefore documented herein. A600E-9149 (abbreviated as A600E) is a Type 1 quaternary ammonium, gel polystyrene resin and has previously been used for Cr(VI) treatment in both pilot- and field-scale applications.[20,21] Trials with other resin types were unsuccessful and described in ESI Text 3.1.†

2.2 NZVI-A600E synthesis

2.2.1 Screening experiments. Prior studies that synthesized NZVI on SBA-IX resin used a variety of procedures, which indicates a lack of methodological consensus, as described in ESI Text 2†.[33,36–41] Based on the variability observed between prior work, 28 screening experiments were performed assessing the following synthesis variables: concentration and volume of $FeCl_3$ and $NaBH_4$, concentration of reagents (*i.e.*, HCl and ethanol) that convert $FeCl_3$ to $FeCl_4^-$, stir time, order of reduction (*i.e.*, $NaBH_4$ before $FeCl_3$), resin mass and type (*i.e.*, A600E, TP 107, A500Plus, and S106), temperature of reaction, method of $NaBH_4$ addition (*i.e.*, titration of $NaBH_4$ into resin suspended in solution *versus* addition of $FeCl_4^-$-resin into $NaBH_4$ solution), $FeCl_4^-$-resin rinsing reagent (*i.e.*, water *versus* ethanol), and resin drying methods. Ultimately, these screening experiments narrowed the test matrix to one resin of interest (*i.e.*, A600E) and eliminated potential synthesis variables based on feasibility before optimization. Outcomes are summarized in ESI Text 3.1.†

2.2.2 Optimization of iron loading. Once initial screening experiments were complete and the hybrid strong base anion exchanger with nanoscale zero valent iron (NZVI-resin) could be synthesized reproducibly, designed experiments were conducted to create an isotherm describing $FeCl_4^-$ loading (eqn (2)). The theoretical mass of iron that could be loaded was 82 mg Fe per g A600E (using the manufacturer-reported resin specifications for minimum capacity and bulk specific gravity). Based on this estimated potential loading, different combinations of iron concentration and volume were tested that spanned the expected iron loading range using a face-centered, central composite design, as shown in Fig. 1A.

To test each of the nine conditions, 1 g of dry A600E resin was stirred at 100 rpm in a small beaker with 20–40 mL containing 0.05–0.1 M Fe^{3+} and 0.1–0.2 M HCl in ethanol solution on a hotplate set at 70 °C for 12 hours. HCl concentration was always maintained at twice the iron concentration to ensure excess chloride conditions. After equilibrium, the resin was removed from the beaker and vacuum filtered with 5 rinses of 5 mL absolute ethanol to remove impurities and excess iron on the resin. After ethanol rinsing, the resin was air dried at room temperature for 24 hours. All nine conditions were tested in duplicate ($n = 2$), and uncertainty is presented as the standard error.

Iron loading onto the $FeCl_4^-$-A600E was analyzed by acid digestion. To measure the solid phase concentration of iron on the resin, 0.1 g of dry $FeCl_4^-$-A600E was digested in 50 mL of 2% HNO_3 solution for 24 hours. The resin visibly leached iron,

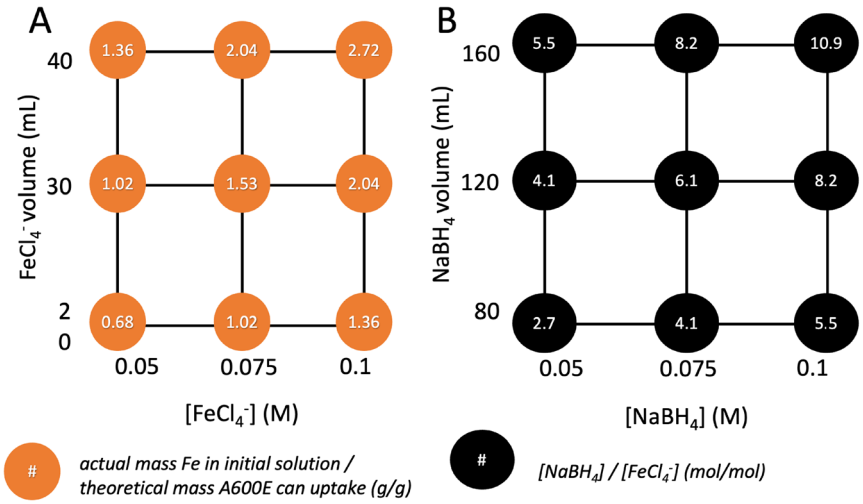

Fig. 1 Face-centered, central composite designs for synthesis optimization. (A) Iron loading test matrix for $FeCl_4^-$-A600E (B) sodium borohydride reduction test matrix for NZVI-A600E.

returning to its original dull yellow color. The iron concentration in solution was quantified to calculate mass of iron that had been exchanged onto the resin.

2.2.3 Optimization of iron reduction. After loading iron onto $FeCl_4^-$-A600E, the next step was to determine the optimal concentration and volume of $NaBH_4$ needed for the reduction reaction (eqn (3)). Enough $NaBH_4$ was needed to reduce all Fe^{3+} to Fe^0; however, too much $NaBH_4$ can have negative practical implications, discussed further in Section 3.4. Theoretically, a 3 : 4 $NaBH_4$: Fe molar ratio is required for NZVI to form. Practically, however, $NaBH_4$ has been added in a 3 : 1 or 4 : 1 $NaBH_4$: Fe molar ratio in other studies.[33,37,38,42] Thus, based on literature, $NaBH_4$: $FeCl_4^-$ molar ratios from 2.7 : 1 to 10.9 : 1 were tested using the face-centered, central composite design shown in Fig. 1B.

To test each of the nine conditions, 80–160 mL of water was purged of dissolved oxygen (DO) using a balloon filled with nitrogen gas (N_2(g)) in a round-bottom, three-neck flask on a hotplate set at 50 °C for 30 minutes (Fig. S10A†). $NaBH_4$ was added to create the 0.05–0.1 M $NaBH_4$ solution. 1 g of dry $FeCl_4^-$-A600E was dropped directly into the $NaBH_4$ solution and stirred at 200 rpm for 15 minutes. The iron reacted with the borohydride, forming what were presumed to be hydrogen gas (H_2(g)) and NZVI on the resin. After the reaction had completed, the solution cleared. The solution was decanted and the resin, now black and magnetic, was vacuum filtered and rinsed with 150 mL of deoxygenated water and 5 mL absolute ethanol. Resin was vacuum dried at room temperature for 48 hours prior to characterization and experimentation. All nine conditions were tested in duplicate ($n = 2$), and uncertainty is presented as the standard error.

After drying the NZVI-A600E, four tests were performed on each of the nine resin conditions. Chromium uptake and pH increase were tested in duplicate ($n = 2$) using an equilibrium batch test. Resin cracking and gas release were evaluated for one of the resin aliquots. For the batch test, 100 mg of dry NZVI-A600E resin was weighed and placed in a 25 mL solution of 175 mg L^{-1} Cr(VI) in 125 mL plastic bottles. Initial pH of the solution was measured. The bottles were placed at room temperature on a shaker table for 24 hours and sampled to quantify chromium. The mass of Cr(VI) removed from solution was calculated by subtraction using the initial and final concentrations measured in solution. All batches were performed in duplicate for each of the nine conditions. The pH after 24 h was measured to calculate the pH change over the course of the experiment. To visually observe cracking, dissecting microscopy was used to quantify breakage by counting approximately 150 resin beads and recording the number of cracked or broken beads relative to the total number counted. To visually observe gas production, 0.2 g dry NZVI-A600E was placed in 10 mL of deoxygenated water for 24 h.

2.2.4 Complete synthesis procedure. After optimizing key synthesis variables, the following methodology was used for material characterization, batch isotherm development, and column experimentation. First, 10 g of dry A600E resin was stirred at 200 rpm in a round bottom flask with 400 mL of 0.05 M Fe^{3+} and 0.1 M HCl in ethanol solution on a hotplate set at 70 °C for 12 hours, allowing Fe^{3+} to exchange onto the SBA-IX resin as $FeCl_4^-$. After the exchange step was complete, the resin was removed from the flask and vacuum filtered with 5 rinses of 50 mL absolute ethanol to remove excess iron from the resin.

After ethanol rinsing, the resin was air dried for 24 hours. Next, 1200 mL water was purged of DO using a balloon filled with N_2(g) in a covered 2000 mL beaker on a hotplate set at 50 °C for 30 minutes (Fig. S10B†). Solid $NaBH_4$ was added to create a 0.1 M $NaBH_4$ solution. Then, 10 g of dry $FeCl_4^-$-A600E was dropped directly into the $NaBH_4$ solution and stirred at 200 rpm for 15 minutes. The iron immediately reacted with the borohydride, forming a gas (presumably H_2(g)) and a solid iron phase (presumably NZVI) on the resin.

After the reaction had completed, the solution was clear with low turbidity. The solution was decanted and the resin, now black and magnetic, was vacuum filtered and rinsed with 300 mL of deoxygenated water and 50 mL of absolute ethanol. Resin was either vacuum dried prior to characterization and

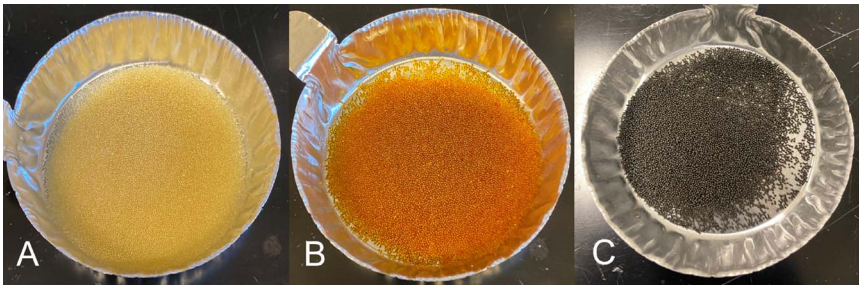

Fig. 2 Photographs of resin at different synthesis steps, including (A) pristine A600E (B) $FeCl_4^-$-A600E (C) NZVI-A600E.

batch experiments or stored in deoxygenated water prior to column experiments. The visual progression through each step is shown in Fig. 2. The pristine A600E resin was dull yellow, the $FeCl_4^-$-A600E was bright orange, and the NZVI-A600E was black in color.

2.3 Batch isotherm experimentation

To test resin capacity and selectivity, equilibrium batch experiments were performed using the resin synthesized according to the methodology in Section 2.2.4. NZVI-A600E was soaked in deoxygenated, 2 N NaCl solution for 30 minutes after synthesis to load exchange sites with chloride, followed by rinsing with deionized (DI) water. A600E, which was delivered in chloride form, was air-dried and NZVI-A600E was vacuum dried for 48 hours. Batch tests used dry resin masses ranging from 50 to 400 mg; the difference in density between A600E and NZVI-A600E resin was corrected for later. Cr(VI) capacity was compared between resins using a solution of 175 mg L^{-1} Cr(VI) created from the $Na_2CrO_4 \cdot 4H_2O$ stock solution. To assess selectivity over sulfate, a binary solution was created composed of 175 mg L^{-1} Cr(VI) and 2000 mg L^{-1} SO_4^{2-} using the $Na_2CrO_4 \cdot 4H_2O$ stock solution and Na_2SO_4(s), respectively. Each isotherm test condition was tested in 125 mL plastic bottles using 25–100 mL of solution and the appropriate mass of dry resin. Even though pH is expected to increase due to excess $NaBH_4$ (*vide infra*), the pH was not adjusted using an acid during batch testing to avoid changing the anionic composition of the solution. To assess the implication of pH variability, the initial pH of each bottle was measured shortly after resin addition. For tests with the pristine resin, initial pH was 8.3–8.6 and increases were <0.2 units during testing. For tests with NZVI-A600E, initial pH was systematically higher and the pH change was greater for samples with the highest resin-to-liquid ratio (up to 0.8 pH increase). The bottles were agitated at room temperature on a shaker table for 24 hours and sampled to quantify chromium. The mass of Cr(VI) removed by the resin was calculated by subtraction using the initial and final concentrations in solution. All batches were performed in duplicate, and uncertainty is presented as the standard error.

Non-linear regressions were fit using the nonlinear specialized modeling tool in JMP Pro 15 for either Langmuir or Freundlich isotherm models shown in eqn (4) and (5).[43]

$$\text{Langmuir: } q_i = \frac{q_{max} K_L c}{1 + K_L c} \quad (4)$$

$$\text{Freundlich: } q_i = K_F c^{1/n} \quad (5)$$

In these equations, q_i is the resin-phase concentration of constituent i, c is the equilibrium liquid-phase concentration, and K_L, q_{max}, K_F, and n are empirically fitted constants. A residuals analysis assessed model adequacy (*e.g.*, absence of systemic patterns, randomness) to identify which empirical model best fit the experimental data across the design space. For the best-fit model, uncertainty on model parameters was calculated using joint probability confidence regions to determine if the modified resin exhibited statistically significant differences in chromium removal. See ESI Text 1.2† for more details.

2.4 Resin density change

The impact of resin form (*i.e.*, $FeCl_4^-$-A600E and NZVI-A600E) on resin density was studied in duplicate ($n = 2$). First, 1 g of dry A600E in Cl^- form was stirred in $FeCl_4^-$, rinsed with ethanol, and air-dried according to the synthesis method in Section 2.2.4. The dried resin was then weighed. Next, 1 g of the dry $FeCl_4^-$-A600E resin was reduced to NZVI-A600E, rinsed with deoxygenated water and ethanol, vacuum-dried, and weighed. In order to determine if synthesis impacted the moisture retention of the resin at room temperature, 1 g of dry resin in each form was placed (in duplicate) in the oven at 100 °C overnight and then re-weighed.

2.5 Fluidized bed column experimentation

Bench experiments were performed using a flow-through, fluidized bed column with a synthetic groundwater matrix. An upflow fluidized bed was selected over a downflow fixed bed to prevent gas accumulation in the bed for NZVI resin, as discussed further in Section 3.4. The column had an inner diameter of 10.74 mm, a wet resin volume of 18 mL, and an empty bed contact time (EBCT) of 3 minutes. The influent water quality was selected to simulate a high-sulfate, Cr(VI)-contaminated groundwater, shown in Table 2.

An effluent sample was collected about every 200 BV until 10 μg L^{-1} Cr(VI) breakthrough was reached, according to the anticipated Cr(VI) MCL in the State of California (USA). After the NZVI-A600E column experiment, the resin, termed post-column NZVI-A600E, was harvested in four cross-sections and dried for characterization. Additional details are described in ESI Text 2.5.†

Table 2 Water quality of the synthetic groundwater. Reported uncertainty is standard error for duplicate measurements ($n = 2$). Bicarbonate concentration represents the amount added gravimetrically. The counterion was sodium for all anions

Parameter	Value
CrO_4^{2-}	91 ± 2 μg L^{-1} as Cr
SO_4^{2-}	97.5 ± 0.3 mg L^{-1}
Cl^-	15.0 ± 0.5 mg L^{-1}
NO_3^-–N	4.82 ± 0.02 mg L^{-1}
HCO_3^-	292 mg L^{-1}
pH	8.89 ± 0.01

2.6 Chemical analytical methods

Inductively coupled plasma mass spectrometry (ICP-MS, Agilent 7900) was used to quantify total chromium and iron concentrations in select experiments, using USEPA 6020B method with collision cell gases (helium or hydrogen) to decrease molecular ion interferences. Ion chromatography (IC, Thermo ICS-6000) was used to quantify sulfate, chloride, and nitrate concentrations, using the USEPA 300.1 method. In the iron loading experiments described in Section 2.2.2, liquid phase iron concentrations (Fe^{3+}) were measured using a colorimetric method. Additional details are provided in ESI Text 2.2.†

2.7 Characterization

A Nikon SMZ800 dissecting microscope was used to evaluate resin shape and breakage. To quantify breakage, approximately 150 resin beads were counted and the number of cracked or broken beads was recorded. Scanning electron microscopy-energy-dispersive X-ray spectroscopy (SEM-EDS) were used to evaluate resin shape and map elemental composition on the resin (Hitachi SU8010). Prior to analysis, platinum was sputtered onto the resin forming a surface thickness of 3 nm.

X-ray photoelectron spectroscopy (XPS) was measured with a Kratos Supra X-ray photoelectron spectrometer to verify Fe^0 presence. Survey spectra were used to calculate the atomic percentage of the surface while the high-resolution spectra provided information on elemental chemical state. Scan sweeps and dwell time were increased to increase the signal-to-noise ratio. Charge neutralization parameters were optimized with continuous scans on the carbon 1s peak. The AlK_α X-ray source was operated at 1486.69 kV and 15.00 mA current emission. Survey spectra were acquired from 0–1200 eV with a resolution of 160, while high resolution scan ranges were based off the element being analyzed and a resolution of 20. All spectra were calibrated using a C–C/C–H peak position of 284.8 eV.

3 Results and discussion

3.1 Synthesis trials

Screening experiments were conducted to explore each of the three steps to synthesize NZVI-A600E resin. In the first step, experiments loaded Fe^{3+} on the SBA-IX resin as $FeCl_4^-$ considering the composition of loading solution. Different methods to rinse and dry the resin were evaluated to determine their impact on the final reduction step that formed NZVI using sodium borohydride.

The screening experiments identified several important experimental variables, including the $FeCl_4^-$ solution composition, selection of rinse solutions, order of reduction steps, method of $NaBH_4$ addition, stir time, temperature, and mass of resin used relative to reaction volumes. Fig. 3 shows three key outcomes from the screening experiments. First, it was determined that a solution of 0.1 M $FeCl_3$ and 0.2 M HCl in 100% absolute ethanol would successfully form orange-colored $FeCl_4^-$ on the A600E resin. If 20% ethanol or a solution without HCl were instead used for the iron loading solution, the resin would turn a bright yellow color, shown in Fig. 3A, and would not react with $NaBH_4$ to form NZVI. This result clarifies methodology for future synthesis work. Previous work has suggested multiple reagents and concentrations to impregnate NZVI on SBA-IX, including 0.5 M $FeCl_3$ with 1 M HCl,[38] 2 M $FeCl_3$ and 2 M HCl,[36] 0.005 M $FeCl_3$ and 0.01 M HCl in ethanol,[37] and 1 M HCl with 10% ethanol, ample NaCl, and 1 M $FeCl_3$.[40] For strong base gel polystyrene resins, such as A600E, the discussed combination of $FeCl_3$, HCl, and 100% absolute ethanol is favorable to form $FeCl_4^-$. As a possible explanation for the importance of ethanol, strong base resins not only swell more in ethanol compared to water but the invasion of HCl into the anionic resin increases as well.[44] In an aqueous matrix, exclusion of HCl may adversely impact the stability of $FeCl_4^-$.

Second, it was determined that rinsing the $FeCl_4^-$-A600E in DI water led to formation of ferric hydroxide solids, which turned the resin deep red, as shown in Fig. 3B. Resin remained

Fig. 3 Key failed NZVI-A600E synthesis outcomes: (A) A600E after $FeCl_4^-$ loading with 20% ethanol and no HCl, (B) $FeCl_4^-$-A600E after rinsing with water until pH = 7, forming $Fe(OH)_3$(s), (C) NZVI-A600E and NZVI in bulk solution due to lack of $FeCl_4^-$-A600E rinsing in ethanol.

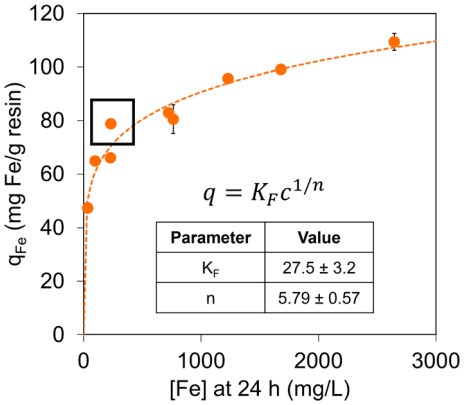

Fig. 4 Isotherm of iron loading onto A600E resin. Model parameters for the Freundlich isotherm are reported in the inset with the 95% confidence limits. Box indicates experimental condition used to optimize reduction conditions. Four points were tested in duplicate. Error bars represent standard error and are smaller than the marker size for two observations. See Fig. S15 and Table S8† for regression uncertainty analysis. Experimental conditions: 1 g of dry A600E resin in chloride form, 20–40 mL of 0.05–0.1 M Fe^{3+} and 0.1–0.2 M HCl in ethanol solution as specified in Fig. 1A, stirred at 100 rpm and 70 °C for 12 hours.

predominantly red after $NaBH_4$ reduction, instead of being reduced to NZVI. Previous work has suggested that rinsing $FeCl_4^-$-resin in DI water until the rinsate measured pH = 7 would prevent bulk solution aggregation of NZVI.[37] However for A600E, this rinse converted $FeCl_4^-$ into unwanted ferric hydroxides.

Third, if $FeCl_4^-$-A600E was not adequately rinsed with absolute ethanol and dried prior to reduction with $NaBH_4$, NZVI also formed in the bulk solution and adhered to the resin, as shown in Fig. 3C. Whereas other literature suggested titrating a solution containing BH_4^-,[33,41] our work determined that dropping dried $FeCl_4^-$-A600E directly into a $NaBH_4$ solution was best for preventing NZVI formation in the bulk solution.

To determine the potential range of $FeCl_4^-$ concentrations that could be loaded onto the resin, an isotherm was created, shown in Fig. 4. A Freundlich adsorption isotherm model best described the data and was fit, where K_F and n are empirical constants.[43] Additional statistical details are provided in ESI Text 3.3 (Fig. S15 and Table S8†). A notable observation is that all the experimental conditions fit the same isotherm regardless of the initial $FeCl_4^-$ concentration. Ion exchange resins swell or shrink with changes in solution osmotic pressure, which impacts the resin hydration and distribution of ions at equilibrium.[22] With the $FeCl_4^-$ concentration varying by a factor of 2 (Fig. 1A) with a proportional HCl molar ratio (2 : 1), the overall ionic strength doubled, but the isotherm did not bifurcate based on initial concentration. Unlike isotherms conducted in aqueous matrices, iron was loaded in an ethanol solution, which has previously shown to swell strong base resin relative to water.[44] Therefore, using ethanol as the solvent, iron loading was not sensitive to iron (or HCl) concentration within this moderate range.

In order to select a test condition (*i.e.*, concentration and volume combination in Fig. 1A) on the isotherm for $NaBH_4$ reduction experiments, a condition in the middle of the isotherm was chosen. The highest iron conditions on the isotherm were avoided to prevent overloading the resin with $FeCl_4^-$, which could have been the cause of iron leaching into solution and formation of aqueous NZVI instead of NZVI formation on the resin during synthesis screening experiments. Thus, the 0.05 M Fe with 40 mL Fe solution per g A600E condition was selected for further experimentation, shown in the box in Fig. 4. The calculated iron loading rate of 78.8 ± 0.6 mg Fe per g resin agreed with the expected theoretical iron loading of 82 mg Fe per g resin discussed in Section 2.2.2. Fig. 4 highlights that the amount of iron loaded prior to reduction can be varied systematically, which may impact material characteristics after reduction. Since reporting the mass of $FeCl_4^-$ initially loaded is not common in other studies, including this measure could benefit inter-study comparisons in future work.

Once the iron loading condition was selected, the $NaBH_4$ concentration and volume for the reduction reaction were varied (Fig. 1B) with a goal to minimize resin cracking, maximize batch Cr(VI) removal, and minimize the increase in pH. Experimental results are shown in Table 3. Resin cracking was correlated with $NaBH_4$ dose (molar ratio of $NaBH_4$ to $FeCl_4^-$). The higher the reductant dose, the more the resin was cracked and even broken. Fig. 5 shows images of three of the nine conditions. pH increase was monitored as a surrogate for presence of excess $NaBH_4$, since $NaBH_4$ produces sodium metaborate ($NaBO_2$) according to eqn (6), which is strongly alkaline when hydrated according to eqn (7).[45,46]

$$NaBH_4 + 2H_2O \rightarrow NaBO_2 + 4H_2(g) \quad (6)$$

$$NaBO_2 + 2H_2O \rightarrow H_3BO_3 + NaOH \quad (7)$$

With the exception of one condition, all batch tests using NZVI-A600E increased the pH more than pristine A600E (Table 3). There was no systematic pattern as a function of reductant concentration or molar ratio.

To quantitatively investigate the dependence of cracking upon both $NaBH_4$ concentration and volume, a two-way analysis of variance (ANOVA) was run in JMP Pro 15. Five terms were statistically significant, including both main effects (*i.e.*, $NaBH_4$ concentration and $NaBH_4$: $FeCl_4^-$ molar ratio), both quadratic terms (*i.e.*, concentration × concentration and molar ratio × molar ratio), and the interaction between factors (concentration × molar ratio). The model output and residuals analysis are presented in ESI Text 3.1.† Concentration had the greatest impact on resin cracking. Fig. 6 shows a contour plot of the impact of $NaBH_4$ concentration and molar ratio on cracking. Only physically realistic features (*i.e.* positive resin cracking values) are plotted.

While the results pointed to one condition as optimal to minimize cracking (*i.e.*, the 0.05 M $NaBH_4$ and 80 mL solution per gram resin), there are several reasons this condition was not selected. First, when observed visually and under the dissecting microscope, about 20% of the resin beads were still orange,

Table 3 Impact of $NaBH_4$ synthesis conditions on NZVI-A600E integrity (resin cracking) and batch testing outcome (Cr(VI) uptake and pH change). Reduction test conditions are outlined in Fig. 1B using 1 g of dry $FeCl_4^-$-A600E resin as described in Section 2.2.3

[$NaBH_4$] (M)	Reductant : resin ratio (mL $NaBH_4$ per g $FeCl_4^-$-A600E)	Reductant : iron ratio (mol $NaBH_4$ per mol $FeCl_4^-$)	Resin cracked (%)	Cr(VI) uptake (mg Cr(VI) per g resin)[a]	pH increase[a]
0.05	80	2.7	1	30.8 ± 0.5	0.3 ± 0.2
0.05	120	4.1	16	29.9 ± 0.6	0.8 ± 0.1
0.05	160	5.5	19	29.6 ± 0.02	0.79 ± 0.01
0.075	80	4.1	42	28.1 ± 0.2	0.9 ± 0.1
0.075	120	6.1	63	29.6 ± 0.2	0.76 ± 0.07
0.075	160	8.2	67	29.8 ± 0.2	0.72 ± 0.01
0.1	80	5.5	58	29.8 ± 0.6	0.78 ± 0.01
0.1	120	8.2	89	30.5 ± 0.2	0.87 ± 0.01
0.1	160	10.9	80	30.2 ± 0.2	0.77 ± 0.01
Pristine A600E			0	27.43 ± 0.08	0.41 ± 0.03

[a] Experimental conditions for the batch test included 100 mg of dry NZVI-A600E resin, 175 mg L^{-1} Cr(VI) in 25 mL of DI water. Uncertainties listed are standard errors for experiments with $n = 2$.

indicating that not enough $NaBH_4$ had been added to react with all the iron, as shown in Fig. 5A. This test condition was the only NZVI-A600E condition that did not exhibit a pH increase (Table 3). In addition, the standard error of 0.5 mg g^{-1} between duplicate measurements of Cr(VI) uptake for this condition was higher than many of the other tests, decreasing confidence in its reproducibility. Therefore, the condition with the next highest Cr(VI) removal, 0.1 M $NaBH_4$ and 120 mL solution (per gram resin), was selected for batch and column experimentation. Unfortunately, this condition exhibited a large pH increase and high prevalence of resin cracking and breaking, as shown in Fig. 5C. The central composite design approach was expected to find a $NaBH_4$ condition with complete NZVI formation but without the downsides of using excess $NaBH_4$. However, no such condition was found. For the purpose of this work, the condition using 0.1 M $NaBH_4$ and 120 mL $NaBH_4$ solution (per gram resin) was selected for additional characterization.

Cracking occurs when a large difference in osmotic pressure between the resin and liquid phase causes resins to swell.[47–49] Previous work has shown that gel resins, such as A600E, are more susceptible to cracking than macroporous resins due to decreased porosity.[48] Our hypothesis was that since air dried $FeCl_4^-$-A600E resin was added directly into the $NaBH_4$ solution, the shock of simultaneous resin re-hydration and Fe^{3+} reduction to Fe^0 could lead to resin expansion as NZVI formed. This swelling would be accentuated at high $NaBH_4$ doses, which could cause the Fe^{3+} reduction to occur faster. However, when hydrated $FeCl_4^-$-A600E resin was used (instead of air dried resin) or $NaBH_4$ was titrated in as a solid or concentrated solution, suspended NZVI formed in the bulk solution, was challenging to separate out, and oxidized on the resin quickly. Therefore, optimizing the procedure to simultaneously prevent osmotic shock while avoiding NZVI formation in the bulk solution would require further optimization.

Literature is sparse on occurrence of NZVI-substrate cracking. Several papers that synthesized NZVI-resin have documented photographs and SEM images of uncracked NZVI.[37,50] Two studies reported a cracked phosphorylated nanoscale zero valent iron (p-nZVI) that increased mass diffusion through abundant nanochannels, leading to more efficient removal of heavy metals including Cr(VI) as compared to uncracked media.[51,52] Another study by Huang *et al.*, 2023 used phosphorus-doped biochar as a substrate for nanocracked zero valent iron, which was found to improve persulfate and gamma-hexachlorocyclohexane degradation.[53] However, none of these nanocracked zero valent iron studies discussed iron leaching or other negative side effects. Further research could build upon this work to understand the impact of cracking on NZVI performance in column-scale experimentation including intra-particle reactions and effluent water quality.

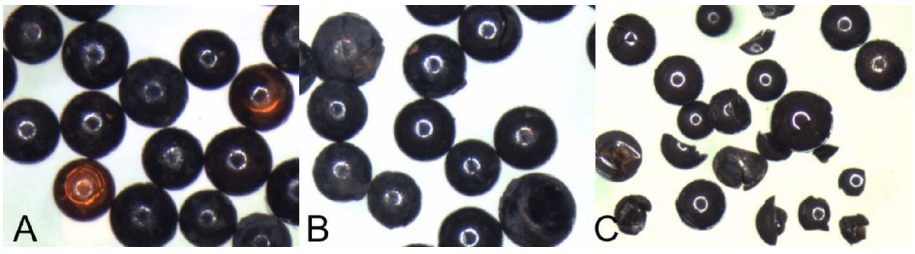

Fig. 5 Dissecting microscopy images of NZVI-A600E over varied $NaBH_4$ conditions: (A) while only 1% of resin was cracked for the 0.05 M and 80 mL $NaBH_4$ condition, some resin beads remained in $FeCl_4^-$ form and had not been reduced. (B) 19% of resin was cracked for the 0.05 M and 160 mL $NaBH_4$ condition. (C) 89% of resin was cracked and broken for the 0.1 M and 120 mL $NaBH_4$ condition.

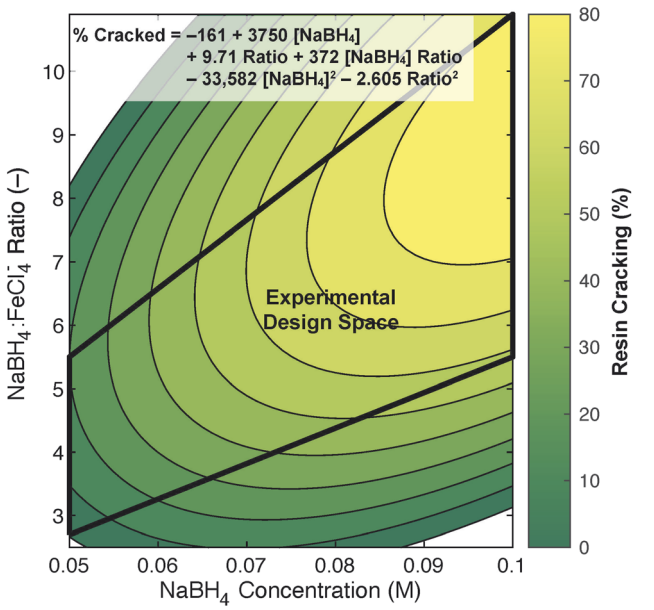

Fig. 6 Contour plot of dependence of resin cracking (%) on $NaBH_4$ conditions with a predicted root mean squared error (RMSE) of 1.62%. Outlined area shows the experimental design space for experimental conditions.

Gas production was not a visually informative dependent variable. Initially, gas was expected only at conditions with excess $NaBH_4$, according to eqn (6). However, gas production occurred at all conditions, including those with less $NaBH_4$ than stoichiometrically required. This observation was likely due to the simultaneous reaction between Fe^0 and H_2O to produce $H_2(g)$, shown in eqn (8):

$$Fe^0 + 2H_2O \rightarrow Fe^{2+} + 2OH^- + H_2(g) \quad (8)$$

Thus, no conclusions about optimal $NaBH_4$ dose were drawn based off of visual gas production. In order to draw conclusions based on this variable, future work could measure the quantity of gas produced to determine if more gas was produced from higher $NaBH_4$ conditions. Since Fe^0 produces gas regardless of the reductant used to synthesize it, the use of NZVI in packed bed systems, which require purging of air bubbles in order to maintain plug flow conditions, may be limited.

The literature confirms that NZVI forms hydrogen gas bubbles in laboratory- and field-scale experiments.[54,55] One study injected NZVI and excess $NaBH_4$ into a cell simulating flow through porous media and found that more gas was produced from higher concentrations of $NaBH_4$ added in conjunction with NZVI.[55] In Johnson *et al.*, 2013, NZVI was pumped into a field-scale aquifer model for groundwater remediation. The experiment found that bubble formation occurred in the reactor and changed the groundwater flow path. Bubble formation was attributed both to the reaction of NZVI with water and the decomposition of residual borohydride.[54] These studies support the results of this work that found NZVI bubbling to be inevitable. While other NZVI-resin studies have omitted mention of this phenomenon, we find it pertinent to evaluate for future novel materials to discuss the practical implications of using NZVI in field applications.

3.2 Resin density change

The impact of resin form on its density has not been previously presented in the literature. Resin density is important because resin capacity in batch experimentation is calculated per mass of dried resin. When the density is different between the same type of resin in two different forms, such as pristine A600E and NZVI-A600E, this difference can bias performance comparisons. The NZVI-A600E resin was approximately 13% heavier than the A600E resin in Cl^- form, as shown in Table S7.† In order to ensure the NZVI-A600E mass gain was not simply due to differences in moisture retention on the resin during air drying, the two dried samples were both put in the oven at 100 °C overnight. When removed from the oven, A600E lost 8.8% mass and NZVI-A600E lost 7.9% mass. A 2-sample *t*-test, assuming equal variances, showed no significant difference is water retention between the A600E and NZVI-A600E ($p = 0.18$), and NZVI-A600E was denser due to the NZVI formation in the particle. This density change would systematically impact batch isotherm results (and therefore Cr(VI) removal) and should be considered as standard practice in future studies.

3.3 Batch experiments

Batch experiments were performed to assess differences in capacity and selectivity between A600E and NZVI-A600E materials. Capacity was compared using Cl^- from resin in a solution containing only Na_2CrO_4. Differences in selectivity were assessed using Cl^- form resin in a solution containing both Na_2CrO_4 and Na_2SO_4. In this study isotherms are compared quantitatively by fitting Langmuir or Freundlich models to determine if there were statistical differences in model parameters. However, these models can only be interpreted as empirical regressions, because the models do not capture the law of mass action constraining ion exchange materials or the dual functionality of hybrid resins (*i.e.*, materials with both ion exchange sites and reaction/sorption sites). For these reasons, isotherm models describing more specific adsorption mechanisms (*e.g.*, Toth, Temkin, Volmer) were not explored.[56] ESI Section 3.3† includes details about statistical analyses for isotherm models. While equilibrium batch experiments are simple and easier to perform than flow through column experiments, this study revealed their drawbacks.

The capacity experiments showed no difference in sorption capacity between NZVI-A600E and A600E (Fig. 7A). Without resin density correction, resin capacity for Cr(VI) appears lower for NZVI-A600E than A600E. When accounting for the 13% resin density increase from A600E to NZVI-A600E in the isotherm, the chromium uptake was indistinguishable between the two resins (78 mg Cr(VI) per g resin), using the experimental condition with an aqueous Cr(VI) concentration between 80–100 mg L^{-1}. The experimental condition at the highest aqueous Cr(VI) concentration was not interpreted due to higher propagated error from small differences in measured aqueous concentration and small resin masses. The A600E isotherm in the Cr(VI)-only

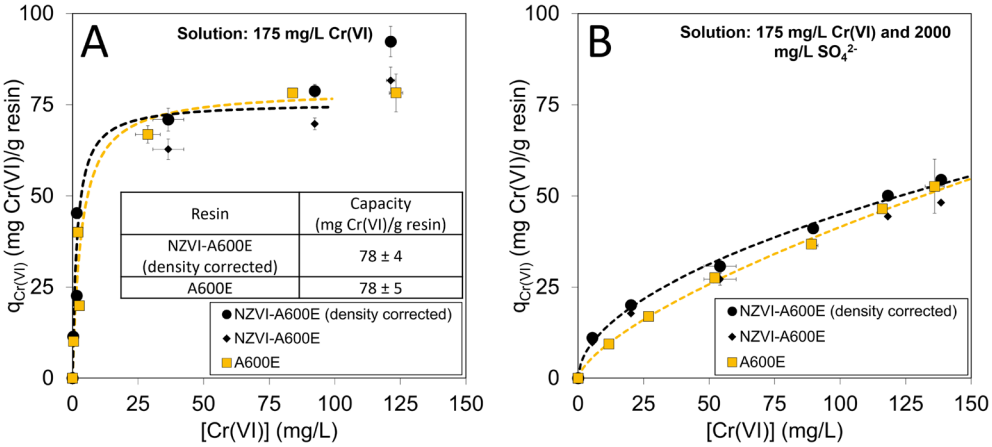

Fig. 7 Batch isotherms for A600E and NZVI-A600E in (A) 175 mg L^{-1} Cr(VI) and (B) 175 mg L^{-1} Cr(VI) with 2000 mg L^{-1} SO_4^{2-}. Isotherms for NZVI-A600E are shown with and without corrections for resin density. Each condition was tested in duplicate. Data are shown as the average value. Error bars represent standard error and may be smaller than the marker size. Isotherm statistical analyses are documented in Fig. S16–S18 and Table S9.† Experimental conditions: Cl-form resin, 50–400 mg dry resin, 25 mL solution, 24 hour agitation.

solution (shown in Fig. 7A) followed a Langmuir-like trend with capacity leveling off with increasing aqueous concentration. With highest concentration included, the data would suggest a Freundlich-like isotherm behavior, but that model would not adequately represent the steep slope at low Cr(VI) concentrations (Fig. S17†). Fitting a Langmuir isotherm with the point excluded, the model fits Cr(VI) removal at lower concentrations better, and the confidence interval on the model parameters suggests no difference in capacity between materials. Equation parameters and joint probability confidence regions are shown in ESI Text 3.3.†

In a solution with a competitive anion (2000 mg L^{-1} SO_4^{2-}), the density-corrected measurements show more Cr(VI) removal at low aqueous phase concentrations with progressively smaller differences in removal between materials as aqueous concentration increases. Freundlich isotherms described the data best, and the 95% joint probability confidence regions were compared for the model parameters. Although there is some overlap in the regions (Fig. S18†), the least-squares model parameters for both K_F and n were greater for NZVI-A600E (K_F = 4.0 $L^{1/n}$ $mg^{(1-1/n)}$ g^{-1}, $n = 1.9$) than A600E ($K_F = 1.8$ $L^{1/n}$ $mg^{(1-1/n)}$ g^{-1}, $n = 1.5$). This difference suggests improved selectivity for Cr(VI) over SO_4^{2-} using NZVI-A600E at lower concentrations.

There is limited information in the literature comparing Cr(VI) removal between unmodified and NZVI-modified anion exchange resin using batch experiments. Gao *et al.*, 2022 performed a 60 minute batch test using 50 mg L^{-1} Cr(VI) at pH = 5.5 and found that NZVI-resin removed over 80% of Cr(VI), while unmodified resin removed just under 60% of Cr(VI).[33] While the study did not consider SO_4^{2-} as a background constituent, it found that coexisting Cl^- had almost no effect on Cr(VI) removal, CO_3^{2-} inhibited Cr(VI) removal, and PO_4^{3-} promoted Cr(VI) removal due to its buffering capacity in water.[33] Another study, Liu *et al.*, 2022, compared phosphorus removal at equilibrium (120 minutes at pH = 7) and reported higher removal for NZVI-resin (24.48 mg P g^{-1}) compared to unmodified resin (16.26 mg P g^{-1}).[37] In an equilibrium batch test with 100 mg L^{-1} SO_4^{2-} and 50 mg L^{-1} P, the NZVI-resin also exhibited higher phosphorous selectivity (20.41 mg P g^{-1}) compared to unmodified resin (11 mg P g^{-1}).[37] However, since this study was targeting P instead of Cr(VI), the comparison is limited.

Overall, batch tests may not be the best measure of resin performance due to experimental constraints that introduce important limitations. Batch tests use Cr(VI) concentrations that are 3 orders of magnitude higher (*i.e.*, 175 mg L^{-1} instead of 100 μg L^{-1}) than expected in groundwater. It is possible that NZVI reacts with high concentrations of Cr(VI) differently than in trace levels. In addition, the test for selectivity over SO_4^{2-} was not representative of trace conditions, since SO_4^{2-} is often 3 orders of magnitude higher concentration than Cr(VI) in groundwater (*i.e.*, 100 mg L^{-1} SO_4^{2-} *vs.* 100 μg L^{-1} Cr(VI)), as opposed to the 1 order of magnitude higher concentrations in the batch test (*i.e.*, 2000 mg L^{-1} SO_4^{2-} and 175 mg L^{-1} Cr(VI)). Fundamental theory also outlines that at trace concentrations, equilibrium capacity is a function of the competitive ions (*e.g.*, sulfate) and not the trace ion (*e.g.*, chromate).[22] Thus, due to the differences in water quality and redox potential, the batch experiments were only a starting point for further column experimentation.

3.4 Fluidized bed column experimentation

Column experiments are better suited than batch experiments for predicting resin performance for drinking water treatment, because a representative water quality uses μg L^{-1} concentrations of Cr(VI) instead of mg L^{-1} levels. Although batch experiments were beneficial for synthesis screening and for an initial comparison of resin capacity and selectivity for Cr(VI) over SO_4^{2-}, column experiments are more relevant to practical applications using a flow-through application with SO_4^{2-} at a thousand times the chromate concentration (approximately 91 μg L^{-1} Cr(VI) and 97.5 mg L^{-1} SO_4^{2-}). Gorman *et al.*, 2016 developed a model for unmodified A600E that predicts throughput to 8 μg L^{-1} Cr(VI) effluent concentration for influent

waters with NO_3^-, SO_4^{2-}, and Cr(VI). That study found that treatment performance was most sensitive to raw water SO_4^{2-} concentration compared to NO_3^- and Cr(VI).[21] While Gorman *et al.*, 2016 tested a limited range of influent water qualities (*i.e.*, 14–49 mg L^{-1} SO_4^{2-} and 12–17 μg L^{-1} Cr(VI)), it can be inferred that breakthrough for the unmodified A600E resin in this work would be well under 12 000 BV, the predicted throughput for about 50 mg L^{-1} SO_4^{2-}.[21]

In the column tests using raw water with 91 μg L^{-1} Cr(VI), the NZVI-A600E resin ran 360% longer to Cr(VI) breakthrough than the A600E resin in the column, as shown in Fig. 8. Effluent concentrations were non-detect for the first 500 BV for A600E and the first 1900 BV for NZVI-A600E. Then, Cr(VI) breakthough, for both A600E and NZVI-A600E, followed an S-shaped curve, which is characteristic of breakthrough curves for favorable isotherms.[57] A comparison endpoint of 10 μg L^{-1} Cr(VI) was chosen, as shown in Fig. 8, because of the anticipated 10 μg L^{-1} MCL in California expected in fall 2024. At this endpoint, A600E treated 800 BV, and NZVI-A600E treated 2880 BV.

In contrast to Cr(VI) breakthrough, both A600E and NZVI-A600E demonstrated the same breakthrough curve for SO_4^{2-} at 800 BV (Fig. 8B). Since SO_4^{2-} and NO_3^- (see ESI† for NO_3^- data) showed similar breakthrough for both resins, the NZVI embedded in the resin did not block ion exchange sites. Illustrated by the 3.6 times increase in Cr(VI) throughput, NZVI was effective at selectively removing Cr(VI) without increasing removal of background constituents such as SO_4^{2-}. This result indicates that the NZVI-resin is favorable for selective Cr(VI) removal for water treatment applications with high SO_4^{2-} in the raw water.

This side-by-side comparison of bench and column studies demonstrates the need to evaluate novel materials for drinking water treatment under realistic conditions. The column experiment showed a large increase in Cr(VI) removal using NZVI-resin compared to unmodified resin, while the batch experimentation only suggested a small difference. The column experiment was performed with Cr(VI) as a trace contaminant (91 μg L^{-1} Cr(VI) and 97.5 mg L^{-1} SO_4^{2-}), whereas the batch experiment tested concentrations of both Cr(VI) and SO_4^{2-} (175 mg L^{-1} Cr(VI) and 2000 mg L^{-1} SO_4^{2-}) with only one order of magnitude difference. When one ion is present at trace concentrations, its isotherm can be described by Henry's Law as a linear isotherm model,[22] which is not representative of batch isotherms using mg L^{-1} concentrations (Fig. 7). Notably, Fig. 7B showed the increasing differentiation in material selectivity as aqueous concentrations decreased. A key outcome of this study is the demonstration of how batch tests do not test conditions that are representative for trace contaminants.

Only two studies identified in literature performed column studies using NZVI-resin for Cr(VI) removal, and both used cation exchange resin, which does not select for anionic chromate.[34,35] There are therefore no other studies with which to directly compare this work. Other works, however, showed twice the throughput in column studies using NZVI-resin compared to unmodified resin to remove contaminants including lead (Pb^{2+}) with no background constituents (4200 BV compared to ~2000 BV) and PO_4^{3-} in the presence of SO_4^{2-}, NO_3^-, and Cl^- (~1850 BV compared to ~900 BV).[37,50] In a more similar application, one study demonstrated a two-fold higher throughput to remove trace concentration of Cr(VI) using an iron sulfide (FeS_2) hybrid anion exchange resin.[58] Our work, therefore, shows continued performance improvements using NZVI-A600E to achieve of 3.6-fold increased throughput compared to the unmodified A600E for Cr(VI) removal in the presence of SO_4^{2-}.

Four factors with potential practical implications were observed during the first 800 BV of the NZVI-A600E resin column experiment: iron leaching, boron leaching, pH increase, and gas bubbling. First, iron leached off the resin into the effluent column water. Fig. 8D shows a plot of iron in the effluent over the course of the run, which decreased below 30 μg L^{-1} by 1000 BV. The USEPA sets a secondary MCL for iron at 0.3 mg L^{-1}. During the first 800 BV of the NZVI-A600E column run, the iron concentration was above the non-enforceable regulatory limit.

Literature on iron leaching from NZVI is limited. Du *et al.*, 2013 performed a fixed-bed column study using polystyrene strong base NZVI-resin. Reported effluent iron concentrations were below 0.1 mg L^{-1} and lower for NZVI-resin than with NZVI only.[59] Another work, Zeng *et al.*, 2022, compared polystyrene strong base NZVI-resin and the same resin with a sulfide-modified NZVI procedure using $NaBH_4$ with sodium dithionite ($Na_2S_2O_4$) (S-NZVI-resin). More iron leached from the NZVI-resin than the S-NZVI-resin in batch adsorption experiments.[60] This phenomenon was hypothesized to occur due to a FeS_x layer that formed on the resin, which inhibited both Fe^0 agglomeration and iron oxide formation and promoted the transfer of electrons.[60] While specific iron concentrations were not mentioned, the study also found that NZVI-resin iron leaching increased the longer the experiment lasted.[60] Understanding the mechanisms and magnitude of iron leaching will be important for full-scale drinking water treatment applications depending on applicable limits.

Second, boron was also detected in the effluent, due to residual boron synthesis reagents (*e.g.*, $NaBH_4$, $NaBO_2$, and H_3BO_3) leaching off the resin. While boron is not federally regulated in drinking water and has not been linked to carcinogenicity, various states in the U.S. (*e.g.*, CA, FL, ME, MN, NH, and WI) have set drinking water guidelines ranging from 0.6–1 mg L^{-1} as B.[61] Fig. 8D shows effluent boron was over 4 mg L^{-1} at the start of treatment and decreased below 50 μg L^{-1} by 1000 BV. Improved synthesis methods would be needed to decrease residual boron for similar materials developed for drinking water applications.

Third, pH of the column effluent was about 0.2 units higher than the raw water after start-up. By 800 BV, pH stabilized to the influent pH value, as shown in Fig. 8C. The initial increase in pH is likely due to residual $NaBH_4$, which forms an alkaline solution (eqn (7)). An increase is opposite from the expected trend that occurs in SBIX processes. As demonstrated by A600E in Fig. 8C, pH dropped below 8 after start-up due to bicarbonate exchanging onto the resin, which can release a H^+ due to the resin favoring carbonate (CO_3^{2-}).[62] Changes in pH can impact corrosion control in drinking water systems.

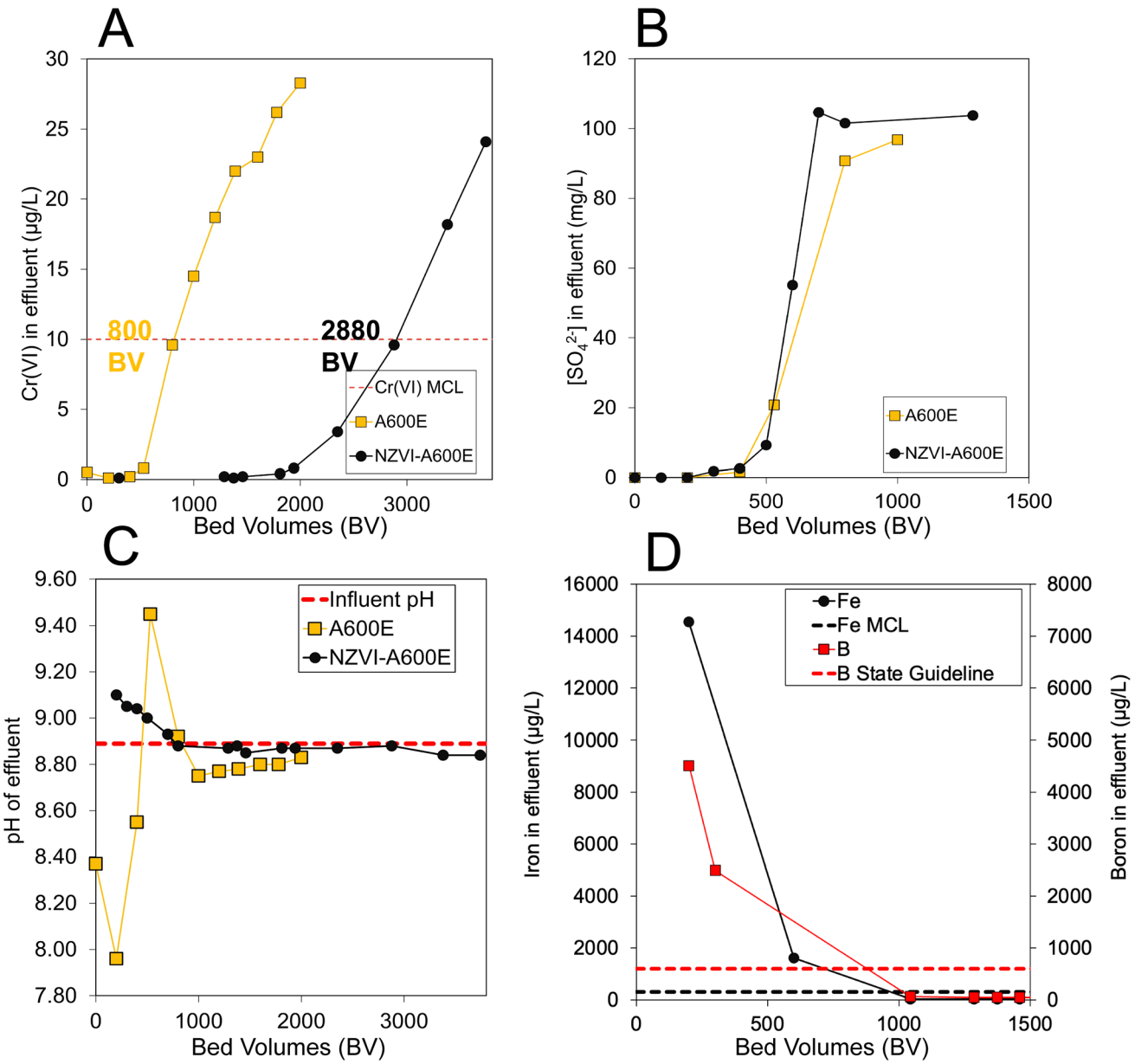

Fig. 8 Breakthrough curves for (A) Cr(VI), (B) sulfate, and (C) pH in comparative upflow column experiments. (D) Iron and boron breakthrough curves in NZVI-A600E upflow column experiments. The state drinking water guideline of 600 µg L^{-1} for boron is shown for Minnesota, USA. Feed water composition is listed in Table 2. Column test conditions: 10.74 mm diameter, 18 mL bed volume (settled resin, wet basis), 3 min EBCT, 6 mL min^{-1} upflow.

Fourth, gas was produced by the NZVI-A600E during loading. It was due to this challenge that the column was operated upflow instead of the standard downflow. Gas bubbles in a downflow packed column bed create side channels for influent water to bypass the packed bed, compromising its plug flow behavior. Hydrogen gas production is hypothesized to have occurred due to the expected reactions of excess $NaBH_4$ with water (eqn (6)) and NZVI with water (eqn (8)). By 800 BV, the resin had stopped bubbling, which coincides with the pH returning to the raw water values.

Boron release, pH increase, and gas formation are interconnected challenges associated with the $NaBH_4$ used for NZVI synthesis. Johnson *et al.*, 2013 measured both H_2(g) bubbling and residual borohydride when NZVI was pumped into a field-scale model aquifer for groundwater remediation.[54] In addition, since $NaBH_4$ produces a $NaBO_2$ solution, which is strongly alkaline when hydrated, the coinciding increase in effluent pH is expected.[45,46] While literature on NZVI itself has documented these concerns, studies using NZVI-resin for bench- and column-scale work have not discussed residual $NaBH_4$ concerns. Further work should be done to investigate mitigation of these problems for hybrid resins synthesized by $NaBH_4$ reduction.

3.5 Characterization

After optimization of iron loading and borohydride reduction, the NZVI-A600E resin, synthesized following the procedure in

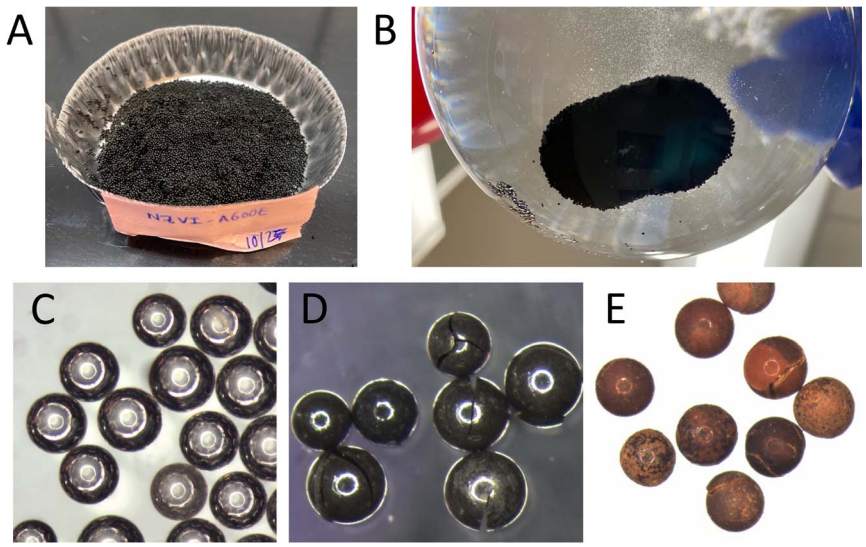

Fig. 9 Photographs of (A) NZVI-A600E resin and (B) NZVI-A600E resin attracted to a metal stir bar in a round bottom flask. Dissecting microscope images of (C) A600E, (D) NZVI-A600E, and (E) post-column NZVI-A600E resins. Images are for visual evaluation rather than quantitative comparison of resin bead size; thus, no scale bar is included.

Section 2.2.4, was characterized using methodology detailed in Section 2.7. Resin collected after column testing was also characterized and is described as "post-column NZVI-A600E" resin.

Resin was first visually inspected. NZVI-A600E was black and magnetically attracted to the metal stir bar, as shown in Fig. 9A and B, agreeing with prior literature.[63] Dissecting microscope images show that the A600E resin was light yellow and uniformly shaped. The NZVI-A600E was black and uniformly shaped; however, some resin beads were cracked. The post-column NZVI-A600E was reddish-brown-orange (Fig. 9C–E).

While many works discuss NZVI oxidation, color change of NZVI-resin during experimentation has surprisingly not been noted in other works. Multiple studies discuss partial oxidation of Fe^0 based on XRD pattern.[33,36,37,59] While not specifically mentioning the color change, Liu *et al.*, 2022 showed a schematic of phosphate adsorption by NZVI-resin with partially oxidized NZVI as a reddish-brown color. This is consistent with the findings of this work, which observed, as shown in Fig. 9D and E, a similar shift from black to reddish-brown-orange during the column study.

3.5.1 SEM-EDS. SEM-EDS in Fig. 10 confirmed the presence of Fe in NZVI-A600E resin beads and showed that these beads were indeed cracked. The EDS recorded 25% Fe on the NZVI-A600E surface and 49% Fe on the post-column NZVI-A600E surface. A similar increase was corroborated by XPS measurements in Fig. 11A. EDS data consistently showed carbon and oxygen (Fig. 10B, C, G, H, L and M), but chlorine decreased after synthesis (Fig. 10D and I) and was not detected after column tests (data not shown). On the post-column resin, there was a layer of reddish-orange solids on the outside of the resin beads shown in Fig. S19C.† EDS analysis of the post-column resin also showed a significant increase in the relative abundance of iron on the surface of the resin (Fig. 10O), which supports the hypothesis that the iron was oxidizing and accumulating on the resin surface. Other works have not reported this increase in Fe abundance on the surface of the resin. Liu *et al.*, 2022 did analyze NZVI-resin after phosphate adsorption using XPS and Fourier Transform Infrared Spectroscopy (FTIR) and noted release of Fe^{2+} due to anaerobic hydrolysis and oxidation to Fe^{3+}, which formed $FePO_4$ on the NZVI-resin.[37] Gao *et al.*, 2022 also noted after reaction with Cr(VI) a change in peaks from Fe^0 to Fe^{2+} and Fe^{3+}, but did not discuss percent composition using EDS.[33] The finding of increased iron on the surface of the NZVI-resin will likely have implications for future assessments of regeneration.

3.5.2 XPS. The XPS full scan identified binding energy peaks at 700 eV (Fig. S20†), indicating the presence of iron on the NZVI-A600E resins. A summary of the atomic composition determined by XPS is shown in Fig. 11A. The unused A600E resin showed peaks for C 1s at 285 eV, O 1s at 531 eV, Cl 2p at 197 eV, N 1s at 400 eV and Si 2p at 101 eV. For the synthesized NZVI-A600E resin, there was an additional Fe 2p peak at 711 eV. After the column test, the C 1s and O 1s peaks persisted but the Cl 2p peak disappeared, likely due to displacement of chloride in the resin by other ions in solution.

Analysis of XPS spectra in the 705–735 eV range indicated zero valent iron was present in NZVI-A600E resin that may oxidize over time. According to literature,[59,64,65] peaks near 706.6 and 719.3 eV correspond to Fe^0, while 710 and 724 eV peaks correspond to oxidized iron valence states (*i.e.*, Fe^{2+} and Fe^{3+}). The NZVI-A600E resin was characterized using XPS the day it was synthesized, 30 days after synthesis, and after column experiments. As shown in the high-resolution Fe scan for the NZVI-A600E resin in Fig. 11B, a small shoulder was observed at 706.6 eV, which can be attributed to Fe^0. The 706.6 eV shoulder was stronger on the day of synthesis sample compared to the sample run 30 days after synthesis. Since the sample

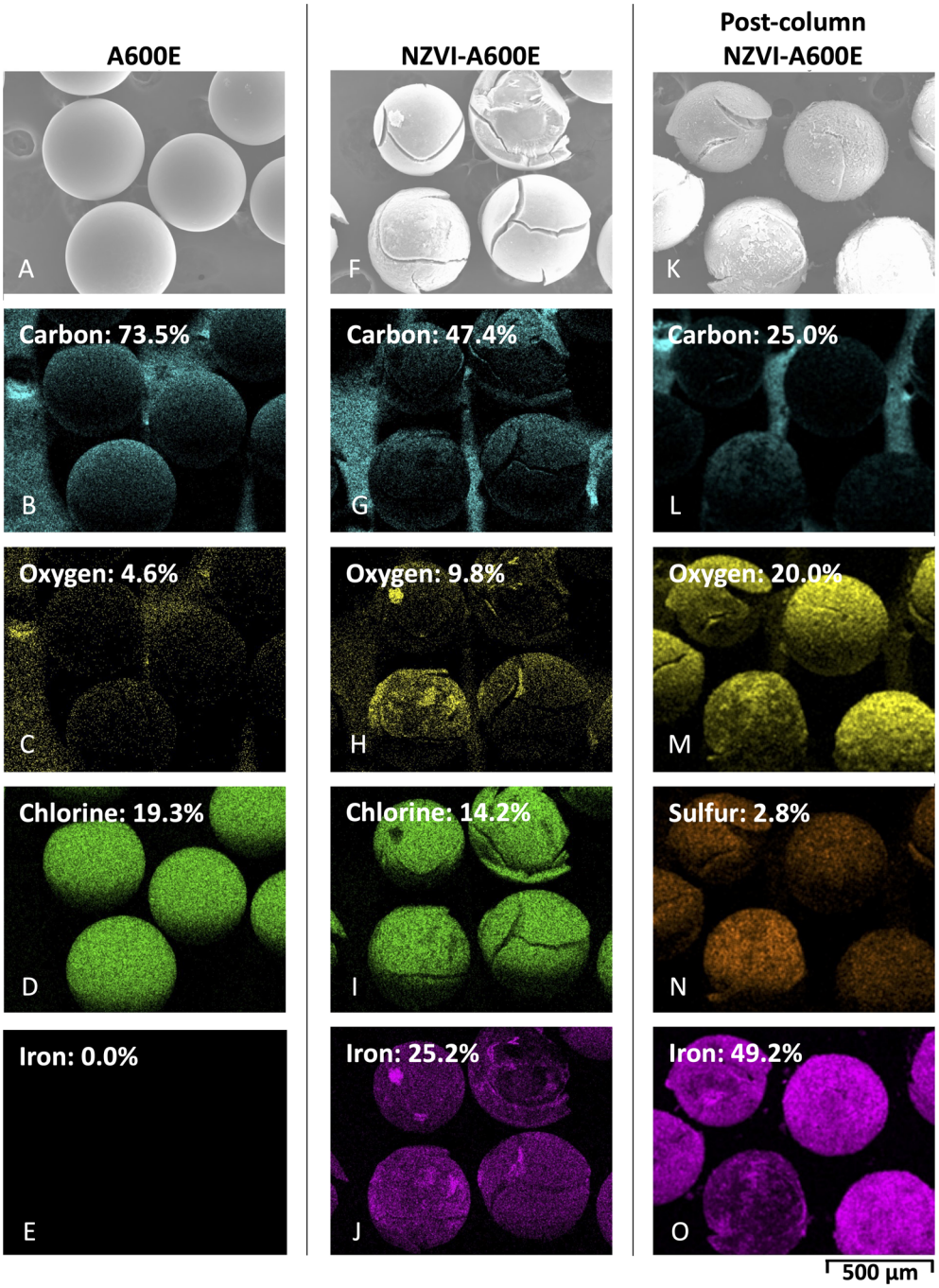

Fig. 10 SEM-EDS image with elemental mapping of (A–E) A600E, (F–J) NZVI-A600E, and (K–O) post-column NZVI-A600E.

characterized 30 days after synthesis shows a decrease in Fe^0 signal, we can conclude that the surface of the resin was oxidized by $O_2(g)$ in air over time, indicating the surface is not stable in air. The lack of 706.9 eV Fe^0 peak in the post-column NZVI-A600E resin in Fig. 11 suggests oxidation of Fe^0 by Cr(VI) or other oxidizing species. Oxidation of Fe^0 does not necessarily preclude effective Cr(VI) removal; the mechanism proposed by Laiju and Sarkar, 2022 suggests nanoparticles in the Fe^{2+} state are also effective for Cr(VI) removal.[58] The atomic composition in Fig. 11A indicates that the relative abundance of iron and oxygen on the resin surface increased after column loading. However, a limitation of XPS characterization is that the penetration depth is limited to about 10 nm, which is small compared to the manufacturer-reported, average resin bead diameter of 570 ± 50 µm. Therefore, oxidation states in the resin core cannot be inferred by XPS.

During the XPS characterization, the NZVI-A600E sample outgassed and required a three hour pump down period for the vacuum to reach pressure. Extensive outgassing was noted during XPS sample introduction in Manning *et al.*, 2007, which

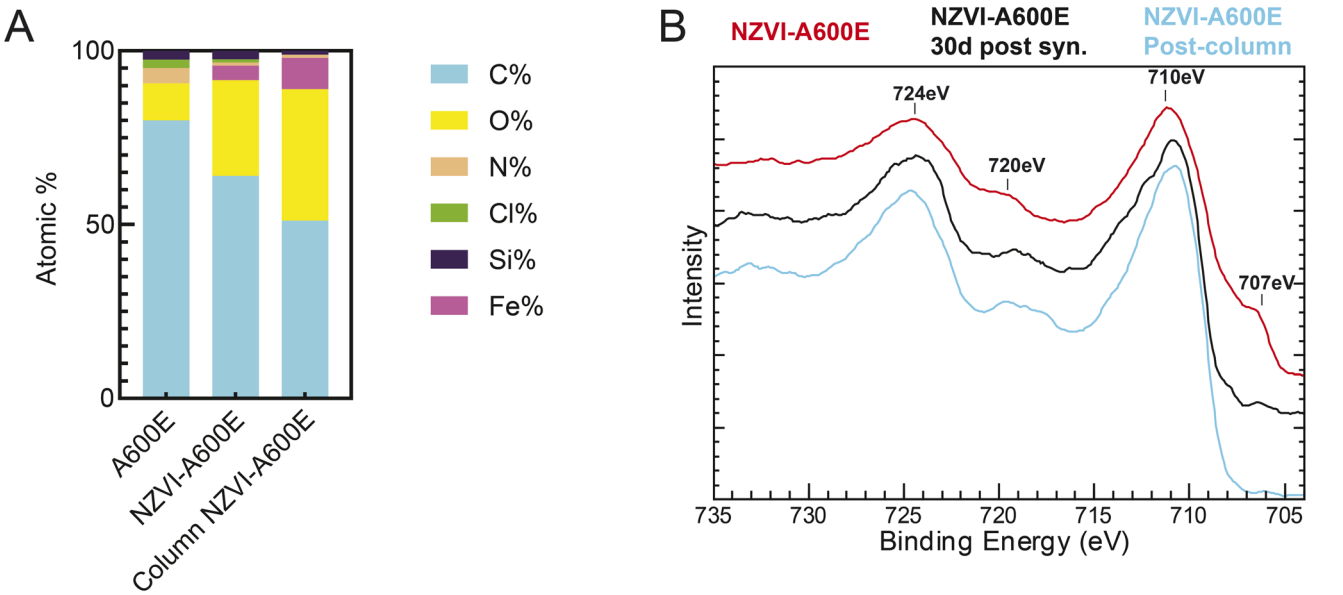

Fig. 11 XPS characterization of A600E and NZVI-A600E resin under different conditions. (A) Atomic composition of A600E and NZVI-A600E resin based on the scans presented in Fig. S20.† (B) XPS scan from 705–735 eV of NZVI-A600E resin. Resin noted as "post-column" was characterized after the column test.

characterized NZVI for Cr(VI) removal.[66] Another work that synthesized NZVI without a substrate degassed the NZVI for 4 hours prior to characterization using an outgassing station to remove adsorbed water and entrapped gasses.[42] This long pumping down period to analyze NZVI-A600E under the XPS vacuum should be noted as challenge. In addition to the possibility of an outgassing station, a cryoscopic technique using liquid nitrogen could be considered for future works.

The relatively weak Fe^0 signal measured by XPS may be explained by the iron oxide shell that typically forms on zero valent iron and geometric effects. Prior studies with NZVI have shown that the surface of the particles forms a shell of iron oxides. Since XPS has a limited penetration depth, the iron oxide shell will appear more pronounced than the Fe^0 core.[67–69] Furthermore, XPS analysis with spherical samples will typically lead to a reduction in peak intensities due to shadowing effects which may make the Fe^0 signal more difficult.[70,71]

4 Conclusions

This work developed a novel Cr(VI) hybrid ion exchanger by synthesizing NZVI on Purolite® A600E strong base ion exchange resin. For NZVI impregnation on anion exchange resin, the most successful synthesis technique included (1) exchanging $FeCl_4^-$ onto resin, (2) rinsing resin with absolute ethanol and air drying, (3) reducing $FeCl_4^-$ by adding the dry resin to a $NaBH_4$ solution under N_2(g) conditions, and (4) desiccating resin under vacuum. Using an upflow fluidized column, NZVI-A600E resin outperformed unmodified resin by 360% for trace Cr(VI) removal. Since the breakthrough curve of SO_4^{2-} and NO_3^- was unchanged between the unmodified and modified resin, the NZVI-A600 resin improved selectivity for Cr(VI) over SO_4^{2-}.

Along with demonstrating the successes of the material, this study also highlighted challenges with synthesis, characterization, and implementation to guide future work in this area. Synthesis methods explored the impact of $FeCl_4^-$ solution composition, selection of rinse solutions, order of reduction steps, and method of $NaBH_4$ addition, among others. Synthesis methods impacted not only the feasibility of forming NZVI in the resin phase but also the integrity of the resin substrate after formation (*i.e.*, materials cracking). It was observed, however, that a successful method for NZVI-A600E resin was not directly transferrable to other commercial resins. This study also illustrated the limitations of relying on batch isotherm testing to assess material advances for trace contaminant removal. Often absent in other HIX studies, this study demonstrated that accounting for the 13% increase in resin density was important for isotherm testing and should be standard practice. Most importantly, batch capacity and selectivity studies did not provide strong evidence that NZVI-A600E would outperform unmodified resin for Cr(VI) removal; however, column testing demonstrated an impactful improvement using representative water qualities. Column studies also revealed challenges with NZVI-A600E that need to be addressed to prevent adverse impacts during water treatment, including leaching of iron and boron, increases in pH, and gas production within the column.

Typically, A600E is used as a regenerable resin for Cr(VI) treatment. For NZVI-resin, a regenerant solution would ideally restore capacity to ion exchange functional groups and reduce the form of iron in nanoparticles for Cr(VI) sorption and reduction. Past work has considered *in situ* regeneration of NZVI by introducing solutions containing HNO_3, $FeCl_3 \cdot 6H_2O$, and $NaBH_4$ synthesis reagents into the column.[50] This study noted iron abundance on the outside of resin increased during loading, suggesting a spatial transport and transformation of

iron that will be important to consider for effective regeneration strategies. Due to the number of variables that would require systematic consideration, further work is needed to understand NZVI-A600E regeneration potential and therefore its suitability for larger scale testing. Both regeneration of NZVI-A600E and preliminary cost analyses were outside the scope of this study.

Overall, this work demonstrated the potential of NZVI-resin for trace Cr(VI) removal. Since other types of hybrid resins have already been commercialized (*e.g.*, ArsenX^{np}), there is an opportunity to leverage the path already forged by resin manufacturers in up-scaling hybrid ion exchange technology to overcome the noted challenges. This work also highlights a need for bench-scale research to prioritize testing under representative conditions, share the successes and failures of synthesis strategies, and characterize the potentially adverse impacts of new materials (*e.g.*, leaching).

Data availability

The data supporting this article have been included as part of the ESI.†

Author contributions

A. M. led the material synthesis, performance testing, and manuscript drafting through the following roles: conceptualization, formal analysis, funding acquisition, investigation, methodology, visualization, writing – original draft, and writing – review & editing. E. H. led the material characterization contributing the following roles: investigation, methodology, visualization, writing – original draft and writing – review & editing. As advisor to E. H., A. S. contributed through supervision and writing – review & editing. As advisor to A. M., J. A. K. contributed through conceptualization, formal analysis, funding acquisition, investigation, methodology, supervision, visualization, and writing – review & editing.

Conflicts of interest

There are no conflicts of interest to declare.

Acknowledgements

A. L. M. and E. A. H. acknowledge support from the NSF Graduate Research Fellowship Program (DGE 2040434). A. L. M. also acknowledges support from the Colorado Groundwater Association through the Harlan Erker Memorial Scholarship. The authors acknowledge Lane Allen for support with dissecting microscopy and Ayush Raj Shahi for support with ion chromatography analysis.

References

1 S. E. Fendorf, Surface reactions of chromium in soils and waters, *Geoderma*, 1995, **67**(1–2), 55–71.
2 D. M. Hausladen, A. Alexander-Ozinskas, C. McClain and S. Fendorf, Hexavalent Chromium Sources and Distribution in California Groundwater, *Environ. Sci. Technol.*, 2018, **52**(15), 8242–8251.
3 C. Oze, D. K. Bird and S. Fendorf, Genesis of hexavalent chromium from natural sources in soil and groundwater, *Proc. Natl. Acad. Sci.*, 2007, **104**(16), 6544–6549.
4 Removal of trace chromate from contaminated water: ion-exchange and redox-active sorption processes, in: *Innovative Materials and Methods for Water Treatment*, ed. Bryjak M., Kabay N., Rivas B. L. and Bundschuh J., CRC Press, 2016, pp. , pp. 353–388. available from: **https://www.taylorfrancis.com/books/9781315682600/chapters/10.1201/b19577-27**.
5 M. Owlad, M. K. Aroua, W. A. W. Daud and S. Baroutian, Removal of Hexavalent Chromium-Contaminated Water and Wastewater: A Review, *Water, Air, Soil Pollut.*, 2009, **200**(1–4), 59–77.
6 R. Saha, R. Nandi and B. Saha, Sources and toxicity of hexavalent chromium, *J. Coord. Chem.*, 2011, **64**(10), 1782–1806.
7 R. M. Sedman, J. Beaumont, T. A. Mcdonald, S. Reynolds, G. Krowech and R. Howd, Review of the Evidence Regarding the Carcinogenicity of Hexavalent Chromium in Drinking Water, *J. Environ. Sci. Health, Part C*, 2006, **24**(1), 155–182.
8 M. Costa, Potential hazards of hexavalent chromate in our drinking water, *Toxicol. Appl. Pharmacol.*, 2003, **188**(1), 1–5.
9 I. Moffat, N. Martinova, C. Seidel and C. M. Thompson, Hexavalent Chromium in Drinking Water, *J. - Am. Water Works Assoc.*, 2018, **110**(5), E22–E35.
10 Official Journal of the European Union, *Directive (EU) 2020/2184 of the European Parliament and Council of 16 December 2020 on the Quality of Water Intended for Human Consumption*, 2020.
11 State Water Resources Control Board, *California Manufacturers and Technology Association and Solano County Taxpayers Association v*, 2017.
12 California Water Boards, *Hexavalent Chromium MCL (SWRCB-DDW-21-003)*, 2023, [cited 2023 Jul 10], available from: **https://www.waterboards.ca.gov/drinking_water/certlic/drinkingwater/SWRCBDDW-21-003_hexavalent_chromium.html**.
13 C. J. Seidel and C. J. Corwin, Total chromium and hexavalent chromium occurrence analysis, *J. – Am. Water Works Assoc.*, 2013, **105**(6), E310–E319.
14 A. Dummer, *Best Available Technologies (BAT) for Hexavalent Chromium Treatment*, California Water Boards, 2021. available from: **https://www.waterboards.ca.gov/drinking_water/certlic/drinkingwater/docs/2022/hexavalent_chromium/pr-request.pdf**.
15 I. Najim, N. P. Brown, E. Seo, B. Gallagher, K. Gramith, N. Blute, *et al.*, *Impact of Water Quality on Hexavalent Chromium Removal Efficiency and Cost*, Water Research Foundation Project, 2014, pp. 1–174, Report No.: 4450.
16 J. C. Crittenden, R. R. Trussell, D. W. Hand, K. J. Howe and G. Tchobanoglous, *MWH's Water Treatment: Principles and Design*, John Wiley & Sons, 2012, p.1921.

17 I. Najim, N. P. Brown, E. Seo, B. Gallagher, K. Gramith, N. Blute, *et al.*, *Impact of Water Quality on Hexavalent Chromium Removal Efficiency and Cost*, Water Research Foundation Project, 2014, pp. 1–174. Report No.: 4450.

18 J. A. Korak, A. L. Mungan and L. T. Watts, Critical review of waste brine management strategies for drinking water treatment using strong base ion exchange, *J. Hazard. Mater.*, 2023, **441**, 129473.

19 S. Plummer, C. Gorman, T. Henrie, K. Shimabuku, R. Thompson and C. Seidel, Optimization of strong-base anion exchange O&M costs for hexavalent chromium treatment, *Water Res.*, 2018, **139**, 420–433.

20 L. C. Flint, M. S. Arias-Paić and J. A. Korak, Removal of hexavalent chromium by anion exchange: non-target anion behavior and practical implications, *Environ. Sci.: Water Res. Technol.*, 2021, **7**(12), 2397–2413.

21 C. Gorman, C. Seidel, T. Henrie, L. Huang and T. Robert, Pilot Testing Strong Base Anion Exchange for CrVI Removal, *J. – Am. Water Works Assoc.*, 2016, **108**, E240–E246.

22 A. K. SenGupta, *Ion Exchange in Environmental Processes: Fundamentals, Applications and Sustainable Technology*, Wiley, 2017, book.

23 S. Sarkar, A. K. SenGupta and P. Prakash, The Donnan Membrane Principle: Opportunities for Sustainable Engineered Processes and Materials, *Environ. Sci. Technol.*, 2010, **44**(4), 1161–1166.

24 K. M. Cross, Y. Lu, T. Zheng, J. Zhan, G. McPherson and V. John, Chapter 24 – Water Decontamination Using Iron and Iron Oxide Nanoparticles, in: *Nanotechnology Applications for Clean Water, Micro and Nano Technologies*, ed. Savage N., Diallo M., Duncan J., Street A. and Sustich R., Boston, William Andrew Publishing, 2009, p. , p. 347–364, available from: **https://www.sciencedirect.com/science/article/pii/B9780815515784500330**.

25 Y. P. Sun, X. qin Li, J. Cao, W. xian Zhang and H. P. Wang, Characterization of zero-valent iron nanoparticles, *Adv. Colloid Interface Sci.*, 2006, **120**(1–3), 47–56.

26 K. Z. Elwakeel, A. M. Elgarahy, Z. A. Khan, M. S. Almughamisi and A. S. Al-Bogami, Perspectives regarding metal/mineral-incorporating materials for water purification: with special focus on Cr(VI) removal, *Mater. Adv.*, 2020, **1**(6), 1546–1574.

27 Y. Han, M. D. Y. Yang, W. Zhang and W. Yan, Optimizing synthesis conditions of nanoscale zero-valent iron (nZVI) through aqueous reactivity assessment, *Front. Environ. Sci. Eng.*, 2015, **9**(5), 813–822.

28 N. C. Mueller, J. Braun, J. Bruns, M. Černík, P. Rissing, D. Rickerby, *et al.*, Application of nanoscale zero valent iron (NZVI) for groundwater remediation in Europe, *Environ. Sci. Pollut. Res.*, 2012, **19**(2), 550–558.

29 K. V. G. Ravikumar, D. Kumar, A. Rajeshwari, G. M. Madhu, P. Mrudula, N. Chandrasekaran, *et al.*, A comparative study with biologically and chemically synthesized nZVI: applications in Cr(VI) removal and ecotoxicity assessment using indigenous microorganisms from chromium-contaminated site, *Environ. Sci. Pollut. Res.*, 2016, **23**(3), 2613–2627.

30 Y. Nomura, D. Inoue and Y. Moritomo, Control of Fe^{3+} coordination by excess Cl^- in alcohol solutions, *RSC Adv.*, 2022, **12**(28), 17932–17936.

31 F. Fu, J. Ma, L. Xie, B. Tang, W. Han and S. Lin, Chromium removal using resin supported nanoscale zero-valent iron, *J. Environ. Manage.*, 2013, **128**, 822–827.

32 A. Toli, K. Chalastara, C. Mystrioti, A. Xenidis and N. Papassiopi, Incorporation of zero valent iron nanoparticles in the matrix of cationic resin beads for the remediation of Cr(VI) contaminated waters, *Environ. Pollut.*, 2016, **214**, 419–429.

33 W. Gao, D. Zhong, Y. Xu, H. Luo and S. Zeng, Nano zero-valent iron supported by macroporous styrene ion exchange resin for enhanced Cr(VI) removal from aqueous solution, *J. Dispersion Sci. Technol.*, 2022, **43**(8), 1197–1207.

34 A. Toli, Ch Mystrioti, A. Xenidis and N. Papassiopi, Continuous Flow Process for Cr(VI) Removal from Aqueous Solutions Using Resin Supported Zero-Valent Iron, *Bull. Environ. Contam. Toxicol.*, 2021, **106**(3), 409–414.

35 A. Toli, C. Mystrioti, I. Avgoustidis and N. Papassiopi, Fixed-bed flow experiments with supported green nZVI for the remediation of contaminated waters: Effect of pH and background solution composition, *Chemosphere*, 2021, **279**, 130472.

36 Z. Jiang, L. Lv, W. Zhang, Q. Du, B. Pan, L. Yang, *et al.*, Nitrate reduction using nanosized zero-valent iron supported by polystyrene resins: Role of surface functional groups, *Water Res.*, 2011, **45**(6), 2191–2198.

37 G. Liu, C. Han, M. Kong, W. H. M. Abdelraheem, M. N. Nadagouda and D. D. Dionysiou, Nanoscale Zero-Valent Iron Confined in Anion Exchange Resins to Enhance Selective Adsorption of Phosphate from Wastewater, *ACS ES&T Eng.*, 2022, **2**(8), 1454–1464.

38 B. Pan, Z. Jiang, W. Zhang, L. Lv, Y. Xie and Q. Zhang. Method for regulating the distribution of metallic nanoparticles within the resin support, *US Pat.*, US9138737B2, 2015, **https://patents.google.com/patent/US9138737B2/en**.

39 Y. Song, Y. Zeng, J. Liao, J. Chen and Q. Du, Efficient removal of sulfamethoxazole by resin-supported zero-valent iron composites with tunable structure: Performance, mechanisms, and degradation pathways, *Chemosphere*, 2021, **269**, 128684.

40 Y. Song, Y. Zeng, T. Jiang, J. Chen and Q. Du, Efficient Removal of Ciprofloxacin from Contaminated Water via Polystyrene Anion Exchange Resin with Nanoconfined Zero-Valent Iron, *Nanomaterials*, 2022, **13**(1), 116.

41 C. Tai, J. She, Y. Yin, T. Zhao and L. Wu, Degradation of 2,4,6-Trichlorophenol Using Hydrogen Peroxide Catalyzed by Nanoscale Zero-Valent Iron Supported on Ion Exchange Resin, *J. Nanosci. Nanotechnol.*, 2016, **16**(6), 5850–5855.

42 M. Barreto-Rodrigues, J. Silveira, J. A. Zazo and J. J. Rodriguez, Synthesis, characterization and application of nanoscale zero-valent iron in the degradation of the azo dye Disperse Red 1, *J. Environ. Chem. Eng.*, 2017, **5**(1), 628–634.

43 M. M. Benjamin and D. F. Lawler, *Water Quality Engineering: Physical/Chemical Treatment Processes*, John Wiley & Sons, 2013, p. 906.
44 G. W. Bodamer and R. Kunin, Behavior of Ion Exchange Resins in Solvents Other Than Water – Swelling and Exchange Characteristics, *Ind. Eng. Chem.*, 1953, **45**, 2577–2580.
45 P. Brack, S. E. Dann and K. G. U. Wijayantha, Heterogeneous and homogenous catalysts for hydrogen generation by hydrolysis of aqueous sodium borohydride ($NaBH_4$) solutions, *Energy Sci. Eng.*, 2015, **3**(3), 174–188.
46 *PubChem. Sodium metaborate*[Internet]. [cited 2023 Jul 5]. available from: **https://pubchem.ncbi.nlm.nih.gov/compound/145326**.
47 W. M. Alvino, Stability of Ion-Exchange Resins. 2. Factors Affecting the Stability of Ion-Exchange Resins, *Ind. Eng. Chem. Prod. Res. Dev.*, 1980, **19**, 276–281.
48 W. M. Alvino, M. C. Skriba and R. Kunin, Osmotic shock stability of ion-exchange resins, *Ind. Eng. Chem. Prod. Res. Dev.*, 1983, **22**, 150–157.
49 L. P. McMaster and E. R. Gilliland, Preparation and Characterization of a Modified Ion-Exchange Resin, ACS Publications. American Chemical Society, 1972 [cited 2024 Jun 20], available from: **https://pubs.acs.org/doi/pdf/10.1021/i360041a017**.
50 N. Chanthapon, S. Sarkar, P. Kidkhunthod and S. Padungthon, Lead removal by a reusable gel cation exchange resin containing nano-scale zero valent iron, *Chem. Eng. J.*, 2018, **331**, 545–555.
51 M. Cao and Y. Zhang, Reductive sequestration of Cr(VI) by phosphorylated nanoscale zerovalent iron, *J. Environ. Manage.*, 2024, **352**, 119987.
52 M. Li, H. Shang, H. Li, Y. Hong, C. Ling, K. Wei, *et al.*, Kirkendall Effect Boosts Phosphorylated nZVI for Efficient Heavy Metal Wastewater Treatment, *Angew. Chem. Int. Ed.*, 2021, **60**(31), 17115–17122.
53 P. Huang, P. Zhang, C. Wang, X. Du, H. Jia and H. Sun, P-doped biochar regulates nZVI nanocracks formation for superefficient persulfate activation, *J. Hazard. Mater.*, 2023, **450**, 130999.
54 R. L. Johnson, J. T. Nurmi, G. S. O'Brien Johnson, D. Fan, R. L. O'Brien Johnson, Z. Shi, *et al.*, Field-Scale Transport and Transformation of Carboxymethylcellulose-Stabilized Nano Zero-Valent Iron, *Environ. Sci. Technol.*, 2013, **47**(3), 1573–1580.
55 O. Mohammed, K. G. Mumford and B. E. Sleep, Effects of hydrogen gas production, trapping and bubble-facilitated transport during nanoscale zero-valent iron (nZVI) injection in porous media, *J. Contam. Hydrol.*, 2020, **234**, 103677.
56 J. Wang and X. Guo, Adsorption isotherm models: Classification, physical meaning, application and solving method, *Chemosphere*, 2020, **258**, 127279.
57 A. K. Sengupta, D. Clifford and S. Subramonian, Chromate ion-exchange process at alkaline pH, *Water Res.*, 1986, **20**(9), 1177–1184.
58 A. R. Laiju and S. Sarkar, A novel hybrid ferrous sulfide impregnated anion exchanger for trace removal of hexavalent chromium from contaminated water, *Chemosphere*, 2022, **305**, 135369.
59 Q. Du, S. Zhang, B. Pan, L. Lv, W. Zhang and Q. Zhang, Bifunctional resin-ZVI composites for effective removal of arsenite through simultaneous adsorption and oxidation, *Water Res.*, 2013, **47**(16), 6064–6074.
60 S. Zeng, D. Zhong, Y. Xu and N. Zhong, A novel sulfide-modified nanoscale zero valent iron supported on porous anion exchange resin composite for Cr(VI) effective removal from waste, *Chem. Phys. Lett.*, 2022, **794**, 139494.
61 U.S. Environmental Protection Agency, *Drinking Water Health Advisory for Boron*, U.S. Environmental Protection Agency, 2008, Report No.: 822-R-08–013.
62 A. Chen, L. Wang, T. J. Sorg and D. A. Lytle, Removing arsenic and co-occurring contaminants from drinking water by full-scale ion exchange and point-of-use/point-of-entry reverse osmosis systems, *Water Res.*, 2020, **172**, 115455.
63 Y. C. Lee, K. Lee, Y. Hwang, H. Andersen, B. Kim, S. Lee, *et al.*, Aminoclay-templated nanoscale zero-valent iron (nZVI) synthesis for efficient harvesting of oleaginous microalga, Chlorella sp. KR-1, *RSC Adv.*, 2014, **4**, 4122–4127.
64 W. Gao, D. Zhong, Y. Xu, H. Luo and S. Zeng, Nano zero-valent iron supported by macroporous styrene ion exchange resin for enhanced Cr(VI) removal from aqueous solution, *J. Dispersion Sci. Technol.*, 2022, **43**(8), 1197–1207.
65 J. Shi, S. Yi, H. He, C. Long and A. Li, Preparation of nanoscale zero-valent iron supported on chelating resin with nitrogen donor atoms for simultaneous reduction of Pb^{2+} and NO^{3-}, *Chem. Eng. J.*, 2013, **230**, 166–171.
66 B. A. Manning, J. R. Kiser, H. Kwon and S. R. Kanel, Spectroscopic Investigation of Cr(III)- and Cr(VI)-Treated Nanoscale Zerovalent Iron, *Environ. Sci. Technol.*, 2007, **41**(2), 586–592.
67 H. J. Martin, K. H. Schulz, J. D. Bumgardner and K. B. Walters, An XPS study on the attachment of triethoxsilylbutyraldehyde to two titanium surfaces as a way to bond chitosan, *Appl. Surf. Sci.*, 2008, **254**(15), 4599–4605.
68 X. Mu, B. Yuan, X. Feng, S. Qiu, L. Song and Y. Hu, The effect of doped heteroatoms (nitrogen, boron, phosphorus) on inhibition thermal oxidation of reduced graphene oxide, *RSC Adv.*, 2016, **6**(107), 105021–105029.
69 M. A. V. Ramos, W. Yan, Li X. qin, B. E. Koel and W. xian Zhang, Simultaneous Oxidation and Reduction of Arsenic by Zero-Valent Iron Nanoparticles: Understanding the Significance of the Core–Shell Structure, *J. Phys. Chem. C*, 2009, **113**(33), 14591–14594.
70 C. D. Easton, C. Kinnear, S. L. McArthur and T. R. Gengenbach, Practical guides for X-ray photoelectron spectroscopy: Analysis of polymers, *J. Vac. Sci. Technol.*, 2020, **38**(2), 023207.
71 A. G. Shard, Practical guides for X-ray photoelectron spectroscopy: Quantitative XPS, *J. Vac. Sci. Technol.*, 2020, **38**(4), 041201.